



## RESEARCH ARTICLE

# Dorsal and ventral mossy cells differ in their axonal projections throughout the dentate gyrus of the mouse hippocampus

Justin J. Botterill<sup>1</sup>  | Kathleen J. Gerencer<sup>1</sup> | K. Yaragudri Vinod<sup>2,3,4</sup> |  
David Alcantara-Gonzalez<sup>1</sup>  | Helen E. Scharfman<sup>1,4</sup>

<sup>1</sup>Center for Dementia Research, The Nathan Kline Institute for Psychiatric Research, Orangeburg, New York

<sup>2</sup>Department of Analytical Psychopharmacology, The Nathan Kline Institute for Psychiatric Research, Orangeburg, New York

<sup>3</sup>Emotional Brain Institute, The Nathan Kline Institute for Psychiatric Research, Orangeburg, New York

<sup>4</sup>Department of Child & Adolescent Psychiatry, Neuroscience & Physiology and Psychiatry and the New York University Neuroscience Institute, New York University Langone Health, New York, New York

## Correspondence

Helen E. Scharfman, Center for Dementia Research, The Nathan Kline Institute, 140 Old Orangeburg Road, Building 35, Orangeburg, NY 10962.

Email: helen.scharfman@nki.rfmh.org

## Funding information

American Epilepsy Society; National Institute of Mental Health, Grant/Award Number: R01 MH-109305; New York State Office of Mental Health

## Abstract

Glutamatergic hilar mossy cells (MCs) have axons that terminate both near and far from their cell body but stay within the DG, making synapses primarily in the molecular layer. The long-range axons are considered the primary projection, and extend throughout the DG ipsilateral to the soma, and project to the contralateral DG. The specificity of MC axons for the inner molecular layer (IML) has been considered to be a key characteristic of the DG. In the present study, we made the surprising finding that dorsal MC axons are an exception to this rule. We used two mouse lines that allow for Cre-dependent viral labeling of MCs and their axons: dopamine receptor D2 (Drd2-Cre) and calcitonin receptor-like receptor (Crlr-Cre). A single viral injection into the dorsal DG to label dorsal MCs resulted in labeling of MC axons in both the IML and middle molecular layer (MML). Interestingly, this broad termination of dorsal MC axons occurred throughout the septotemporal DG. In contrast, long-range axons of ventral MCs terminated in the IML, consistent with the literature. Taken together, these results suggest that dorsal and ventral MCs differ significantly in their axonal projections. Since MC projections in the ML are thought to terminate primarily on GCs, the results suggest a dorsal–ventral difference in MC activation of GCs. The surprising difference in dorsal and ventral MC projections should therefore be considered when evaluating dorsal–ventral differences in DG function.

## KEYWORDS

commissural, hilus, molecular layer, virus, GABA, axon, long-range

## 1 | INTRODUCTION

The dentate gyrus (DG) of the hippocampus is considered critical in cognitive and behavioral functions. It also has been implicated in several neurological and psychiatric conditions (Scharfman, 2007b). Dentate granule cells (GCs) are the main excitatory cell type, and form a key relay from the entorhinal cortex to area CA3 (Amaral, Scharfman, & Lavenex, 2007). Inhibitory gamma-aminobutyric acid

(GABA)-ergic interneurons in the DG provide the main source of inhibition to GCs (Houser, 2007). Hilar mossy cells (MCs) are large glutamatergic neurons that innervate both GCs and inhibitory GABAergic neurons within the DG (Scharfman, 2016; Scharfman & Myers, 2012). MCs make up the majority of hilar neurons, and are known for their complex spines called thorny excrescences (Scharfman, 2016; Scharfman & Myers, 2012). They have dendrites mainly in the hilus and their axon projects to locations within the

This is an open access article under the terms of the Creative Commons Attribution-NonCommercial-NoDerivs License, which permits use and distribution in any medium, provided the original work is properly cited, the use is non-commercial and no modifications or adaptations are made.

© 2021 The Authors. *Hippocampus* published by Wiley Periodicals LLC.

DG. Near the cell body the axon makes collaterals that terminate mainly in the hilus. Distal to the cell body the axon terminates at many septotemporal levels. There is also a commissural projection that terminates in the contralateral DG (Scharfman & Myers, 2012). The complex projections of MCs have led to considerable interest in their contribution to DG function.

Numerous studies have documented the MC axon projection (Scharfman & Myers, 2012), but a seminal study used biocytin to label individual MCs *in vivo* and quantify the axon projections (Buckmaster, Wenzel, Kunkel, & Schwartzkroin, 1996). That study found that while ~25% of the MC axon is located in the hilus, over 60% of the axon was distal from the cell body and located in the molecular layer (ML). The majority of the MC axon projected to the inner molecular layer (IML). However, a small fraction of the axon was found in the middle molecular layer (MML) and minimal expression was found in the outer molecular layer (OML). Using electron microscopy, the authors showed that the primary target of long-range MC axons are GCs, supporting the view that MCs primarily activate GCs (Buckmaster et al., 1996; Buckmaster & Schwartzkroin, 1994).

Historically, MCs have been challenging to study due to the lack of specific tools to visualize or manipulate their activity (Scharfman, 2017; Scharfman & Myers, 2012). Technical advances over the past several years have generated specific transgenic mouse lines and viral methods to label MCs and their axons with a high degree of specificity (Scharfman, 2016, 2017). Two of the most widely used mouse lines to study MCs include calcitonin receptor-like receptor (Crlr-Cre) and dopamine receptor D2 (Drd2-Cre) mice. The robust nature of Cre-dependent viral labeling in both of these lines is well documented (Azevedo et al., 2019; Botterill et al., 2019; Jung et al., 2019; Oh et al., 2019; Puighermanal et al., 2015; Senzai & Buzsaki, 2017; Yeh et al., 2018). Several studies have now used these Cre lines to evaluate effects of MC manipulations *in vivo* or *in vitro* (Azevedo et al., 2019; Bernstein et al., 2020; Botterill et al., 2019; Jinde et al., 2012; Jung et al., 2019; Oh et al., 2019; Puighermanal et al., 2015; Senzai & Buzsaki, 2017; Yeh et al., 2018). However, these mouse lines are also useful to address the MC axon projections in the adult mouse. This type of investigation is valuable because past studies mainly used rats, and in addition there can be strong fluorescence of axons after viral targeting in mice (Lanciego & Wouterlood, 2020).

In the present study, we utilized Cre-dependent viral labeling to evaluate the axons of MCs in Crlr-Cre and Drd2-Cre mouse lines. We administered a single viral injection into the dorsal or ventral hilus to determine whether dorsal and ventral MCs differ in their axonal projections. Both dorsal and ventral injections labeled a large number of MCs proximal to the injection site as well as MC axons throughout the septotemporal axis of the DG bilaterally. Surprisingly, dorsal MCs had a remarkably different pattern of axonal projections compared with ventral MCs. Specifically, dorsal MCs had axons that were within the IML and MML of dorsal sections and almost exclusively in the MML of ventral sections. In contrast, ventral MCs had axons within the IML. Notably, the distinct projections of dorsal and ventral MC axons were similar in both ipsilateral and contralateral sections. Taken together, this study provides novel evidence that dorsal and ventral MCs differ

in their anatomical projections and these findings should be considered when evaluating how MCs influence the activity of the DG network.

Notably, during the review of our manuscript, another group independently confirmed some of the anatomical findings reported in the current study (Houser, Peng, Wei, Huang, & Mody, 2020).

## 2 | METHODS

### 2.1 | Animals and genotyping

All experimental procedures were done in accordance with the National Institutes of Health (NIH) guidelines and approved by the Institutional Animal Care and Use Committee (IACUC) at the Nathan Kline Institute. Highly specific targeting of MCs was achieved using *Drd2-Cre<sup>+/-</sup>* and *Crlr-Cre<sup>+/-</sup>* transgenic mice that were graciously provided by Drs. E. Valjent (France) and K. Nakazawa (USA), respectively. Adult male and female mice were used in all studies (age range: 2–5 months). Hemizygous *Drd2-Cre* and *Crlr-Cre* males were bred in-house to wild-type C57BL/6 females. Breeding pairs were fed Purina 5008 rodent chow (W.F. Fisher) and provided 2" × 2" nestlets (W.F. Fisher). Mice were weaned at postnatal Day 25–30 and housed with same-sex siblings (2–4 per cage) in standard laboratory cages with corn cob bedding. Mice were maintained on a 12 hr light–dark cycle with standard rodent chow (Purina 5001, W.F. Fisher) and water available *ad libitum*. Genotyping was performed by the Genotyping Core Laboratory at New York University Langone Medical Center. The mouse line and sex used for each of the experiments is provided in Table S1.

### 2.2 | Stereotaxic surgery and viral injections

Stereotaxic surgery was performed as previously described (Botterill et al., 2019). Mice were anesthetized with isoflurane (5% induction, 1–2% maintenance; Aerrane, Henry Schein) and secured in a rodent stereotaxic apparatus (Model #502063, World Precision Instruments). Buprenex (Buprenorphine, 0.1 mg/kg, s.c.) was delivered prior to surgical procedures to reduce discomfort. Body temperature was maintained at 37°C via a homeothermic blanket system (Harvard Apparatus). The scalp of each mouse was shaved and swabbed with betadine (Purdue Products) and lubricating gel was applied to the eyes to prevent dehydration (Patterson Veterinary). A surgical drill (Model C300, Grobert) was used to make craniotomies for viral injections (all coordinates in reference to bregma). Craniotomies were made over the dorsal hippocampus (–2.1 mm anterior–posterior and –1.25 mm medial–lateral) or ventral hippocampus (–3.4 mm anterior–posterior, –2.7 mm medial–lateral). In a subset of experiments, a craniotomy was made over left dorsal CA3 (–2 mm anterior–posterior and –2.3 mm medial–lateral).

Viral labeling of MCs and MC axons was achieved using the Cre-dependent construct AAV5-EF1a-DIO-eYFP. *Drd2-Cre* mice were used to target either the dorsal or ventral hilus. *Crlr-Cre* mice were primarily used in experiments targeting the dorsal hilus because we

observed that ventral hilar injections resulted in viral expression in a considerable number of CA3 pyramidal neurons, consistent with previous reports (Jinde et al., 2012; Yeh et al., 2018). Viral labeling of principal neurons in the DG or hippocampal CA3 region was achieved using AAV5-CaMKIIa-ChR2(H134R)-mCherry.

Virus was injected using a 500 nl Neuros Syringe (#65457-02, Hamilton Company) attached to the stereotaxic apparatus. For MC targeting experiments, the syringe needle was slowly lowered into the craniotomy made over the dorsal hippocampus (1.9 mm below skull surface) or ventral hippocampus (3.4 mm below skull surface) and 150 nl of virus was injected at a rate of 80 nl/min. In experiments targeting the hippocampal CA3 region, the needle was lowered 2.3 mm below the skull surface and 100 nl of virus was injected at 80 nl/min. In all experiments, the needle remained in place for at least 5 min after the injection to allow for diffusion of the virus before being slowly removed from the brain. The scalp was then cleaned with sterile saline and sutured using tissue adhesive (Vetbond, 3M). Mice were given 1 ml of lactated ringers (s.c.) at the end of surgery to support hydration. Mice were transferred to a clean cage at the end of the surgery and placed on a heating blanket (37°C) until fully ambulatory.

### 2.3 | Perfusions and sectioning

Mice were euthanized 14 days after surgery to evaluate viral expression. Mice were initially anesthetized with isoflurane, followed by urethane (2.5 g/kg; i.p.). Once under deep anesthesia, the abdominal cavity was opened and the subject was transcardially perfused with ~10 ml of room temperature saline, followed by ~20 ml of cold 4% paraformaldehyde in 0.1 M phosphate buffer (PB; pH = 7.4). The brains were extracted and stored overnight at 4°C in 4% paraformaldehyde in 0.1 M PB. The brains were sectioned at 50 µm in the coronal or horizontal plane (Vibratome 3000, Ted Pella) and one of every six sections were selected for labeling (sections 300 µm apart). In a

subset of experiments, the left hemisphere was cut in the coronal plane, and the right hemisphere was cut in the horizontal plane to evaluate commissural projections of MCs. Sections were stored in 24-well tissue culture plates containing cryoprotectant (30% sucrose, 30% ethylene glycol in 0.1 M PB) at -20°C until use (Botterill, Guskjolen, Marks, Caruncho, & Kalynchuk, 2015; Botterill, Nogovitsyn, Caruncho, & Kalynchuk, 2017).

### 2.4 | Immunofluorescence

Immunofluorescence staining was performed on free floating sections as previously described (Botterill et al., 2019). A minimum of five sections per subject were used for immunofluorescence staining. Sections were washed in 0.1 M Tris Buffer (TB; 3 × 5 min each) and incubated in blocking solution consisting of 5% normal goat serum, 0.25% Triton X-100, and 1% bovine serum albumin in 0.1 M TB for 30 min. To better visualize the MC axons, the viral label was amplified by incubating sections with chicken anti-GFP (1:2,000, #ab13970, Abcam) or rabbit anti-mCherry (1:2,000, #167453, Abcam) primary antibodies diluted in blocking solution.

For double labeling experiments, rabbit polyclonal anti-GluR2/3 (1:200, #AB1506, Millipore), mouse monoclonal anti-calretinin (1:750, #6B3, Swant), mouse monoclonal anti-glutamate decarboxylase 67 (GAD67; 1:500, #MAB5406, Millipore), or rabbit polyclonal vesicular GABA transporter (VGAT; 1:300, #131003, Synaptic Systems) were added to the blocking solution containing primary antibodies against GFP and incubated overnight at 4°C on a rotary shaker with gentle agitation (Table 1). On the following day, the sections were washed in 0.1 M TB (3 × 5 min) and then incubated in goat anti-chicken Alexa 488 (1:1,000, #A11039, Invitrogen), goat anti-rabbit Alexa 568 (1:500 to 1:1,000, #A11036, Invitrogen), or goat anti-mouse Alexa 568 (1:500, #A11004, Invitrogen) secondary antibodies for 2 hr. The sections were then washed in 0.1 M TB (2 × 5 min) and

**TABLE 1** Antibody information

Primary antibodies						
Antigen	Host	Clonality	Dilution	Catalog #	Vendor	RRID#
GFP	Chicken	Polyclonal	1:2,000	#AB13970	Abcam	AB_300798
mCherry	Rabbit	Polyclonal	1:2,000	#167453	Abcam	AB_2571870
Calretinin	Mouse	Monoclonal	1:750	#6B3	Swant	AB_10000320
GAD67	Mouse	Monoclonal	1:500	#MAB5406	Millipore	AB_2278725
VGAT	Rabbit	Polyclonal	1:300	#131003	Synaptic Systems	AB_887869
GluR2/3	Rabbit	Polyclonal	1:100	#AB1506	Millipore	AB_90710
Secondary antibodies						
Antibody	Host	Visualization	Dilution	Catalog #	Vendor	RRID#
Alexa 488 anti-chicken	Goat	Fluorescence (488 nm)	1:1,000	A-11039	Invitrogen	AB_142924
Alexa 568 anti-rabbit	Goat	Fluorescence (568 nm)	1:500, 1:1,000 mCherry	A-11036	Invitrogen	AB_10563566
Alexa 568 anti-mouse	Goat	Fluorescence (568 nm)	1:500	A-11004	Invitrogen	AB_2534072

Note: Information is provided about the use of primary and secondary antibodies in this study. The Research Resource Identifier (RRID#) is also provided.

counterstained with Hoechst 33342 (1:20,000, #62249, Thermo Fisher Scientific) diluted in 0.1 M TB. The sections were then rinsed in 0.1 M TB (2 × 5 min), mounted onto gelatin-coated slides and air dried for 30 min. Sections were then coverslipped using Citifluor anti-fade mounting medium (#17970, Electron Microscopy Sciences).

## 2.5 | Image acquisition

Images were acquired with a Zeiss LSM 880 laser scanning confocal microscope and Zen 3.0 software (Zeiss). Photomicrographs were acquired with Plan-Apochromat 10×/0.45 M27, Plan-Apochromat 20×/0.8 M27, or Plan-Apochromat 40×/1.4 Oil DIC M27 objectives. All images were acquired at 8-bit depth with a frame size of 1024 × 1024 or 2048 × 2048 pixels. For high-resolution insets, the Plan-Apochromat 40×/1.4 Oil DIC M27 objective was used with a 1.9× digital zoom. In cases where the region of interest was too large to fit within a single image (e.g., Figure 1c7–c10), tile scans were acquired with automatic stitching enabled in the acquisition software. Immunofluorescence was visualized with preconfigured excitation and emission wavelengths in the acquisition software for Hoechst 33342 (Ex/EM 408/453 nm), Alexa 488/GFP (Ex/EM 488/535 nm), and Alexa 568/mCherry (Ex/Em 561/643 nm). Zen 3.2 Blue Edition software (Zeiss) was used offline to export raw Zeiss image files (CZI format) into TIF format. Figures were made using Photoshop 21.2.3 (Adobe). When brightness and contrast adjustments were applied to a part of a figure, the same adjustments were made to each part of the figure.

## 2.6 | Quantification of MC axons

To quantify potential differences between the axons of dorsal and ventral MCs, GFP+ immunofluorescence was evaluated in the ML across the septotemporal DG. The ML was defined as a region between the outer border of the granule cell layer (GCL) and the fissure (Amaral et al., 2007; Scharfman, 2016; Figure S1). The IML, MML, and OML, subdivisions of the ML were determined by measuring the total width of the ML and dividing it into equal thirds. Note that the IML is located nearest to the GCL border and the OML ends at the hippocampal fissure. In addition to addressing the axon distribution in the IML, MML, and OML, axons were quantified in the upper blade, crest, and lower blade of the DG. These areas are also known as the suprapyramidal blade, apex, and infrapyramidal blade, respectively.

Three measurements were made that are discussed and diagrammed in the Section 3 and Figures. First, we measured the distance we call “inner GFP”, corresponding to the gap that sometimes occurred between the GCL/IML border and the nearest signal of the GFP+ axon terminal plexus. The gap was measured as the distance from the GCL border with the IML to the edge of the terminal plexus closest to the GCL. Next, we measured a distance we called “outer GFP” which corresponded to the distance from the GCL/IML border to the edge of the GFP+ terminal plexus furthest from the GCL. Finally, we measured the width of the GFP+ signal (i.e., the distance

between the inner and outer GFP+ immunofluorescence in the ML). A schematic of measurements is shown in Figure 5b3.

The distance measurements were made using the “distance tool” in the software program Zen 3.2 Blue (Zeiss). The length feature of the distance tool allows users to draw lines between two points to determine the distance between those points. These lines can be drawn in parallel, leading to the most precise measurements. To define the GCL border with the IML, a line was drawn along the GCL border, defined by Hoechst counterstain. The two edges of the GFP+ axon terminal plexus were defined readily because the plexus was a dense band of GFP+ puncta (reflecting MC axon boutons) and axons that together made a band of immunofluorescence with sharp edges. Since the width of the ML varies across the septotemporal axis and across different blades (e.g., upper vs. crest vs. lower), we normalized distance measurements as a percentage of the total ML width by dividing our measurement of interest by the total width of the ML.

Mice were injected in either the dorsal or ventral hilus and all analyses were done using horizontal sections because of their ability to clearly show the layers of the DG. In contrast, caudal DG in the coronal plane does not show the sublayers of ventral DG as well. A minimum of three dorsal and three ventral sections were analyzed for each subject. We also evaluated the approximate dorsal–ventral locations of our sections using interaural values from a horizontal atlas based on adult C57BL/6 mice. We estimate our sections range from approximately 2 mm interaural at the most temporal level and 6 mm interaural at the most dorsal level, but note that this estimate is approximate because the atlas we used (the mouse brain library, [www.mbl.org/atlas](http://www.mbl.org/atlas)) mentions shrinkage of ~24% should be taken into account. We did not observe any notable difference between ipsilateral and contralateral sections (Table 2) and therefore the values from ipsilateral and contralateral sections were averaged. Experimenters were blinded for all quantitative analyses.

## 2.7 | Data analysis and statistics

All results are presented as the mean ± standard error of the mean (SEM). Statistical comparisons were made using Prism 8.4 (GraphPad) with statistical significance ( $p < .05$ ) denoted on all graphs with an asterisk. Two-way ANOVAs were used for analyzing parametric data with multiple comparisons. Tukey's post hoc test with corrections for multiple comparisons was used when appropriate.

## 3 | RESULTS

### 3.1 | GFP+ expression of MCs following a single dorsal hilus injection

#### 3.1.1 | Coronal sections

Brains were sectioned in the coronal plane across the septotemporal axis of the DG (Figure 1a1,a2) to evaluate viral expression following a



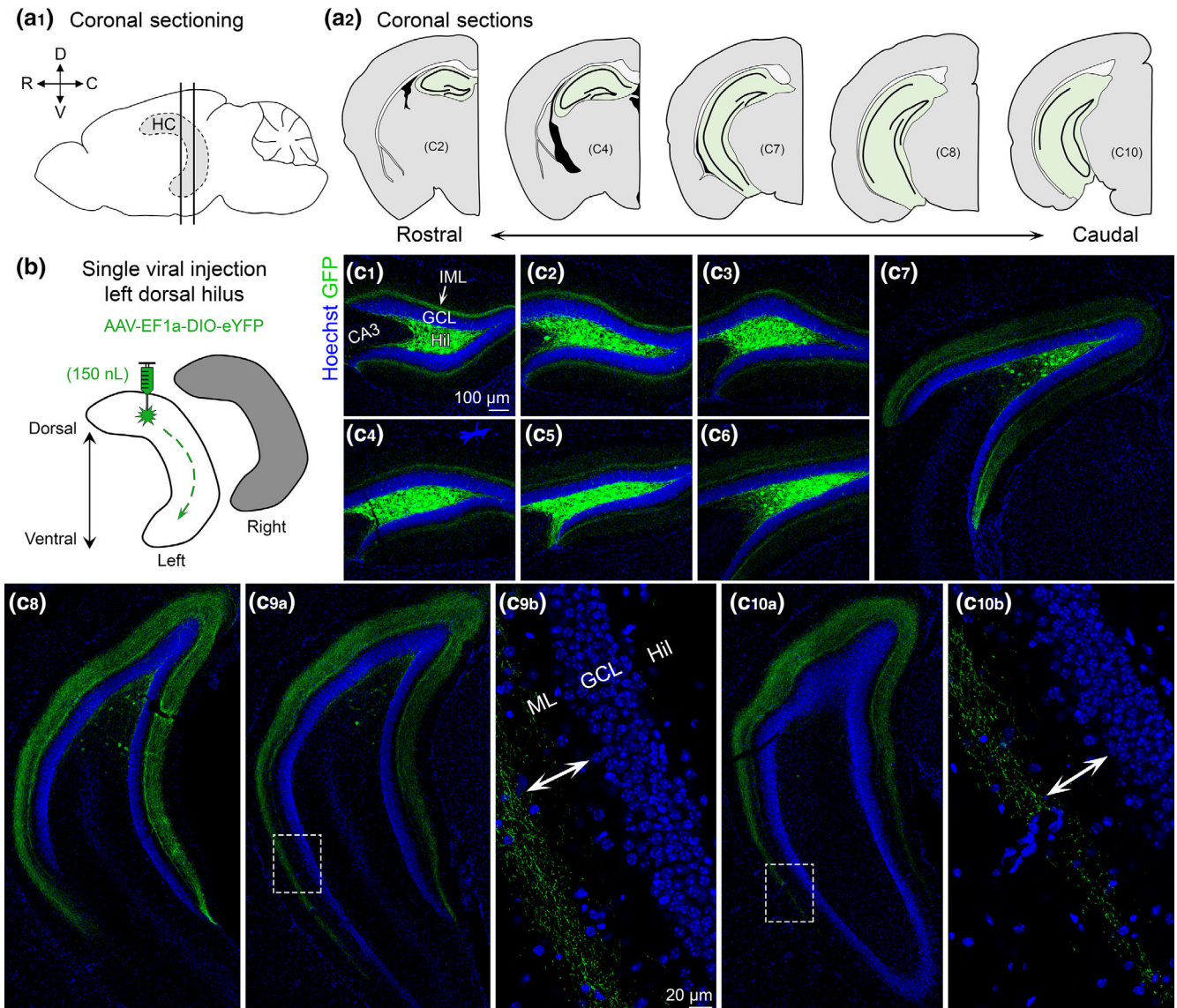


**FIGURE 1** Viral expression of dorsal MCs and axons across the septotemporal axis of the DG. (a1) Side view of the brain showing the hippocampus (HC; grey with dashed border). Straight vertical lines are shown to depict sectioning in the coronal plane. (D) Dorsal, (V) Ventral, (R) Rostral, and (C) Caudal. (a2) Representative schematic of coronal sections starting from the rostral pole and extending to caudal hippocampus (green). (b) Viral injection schematic. 150 nl of AAV-EF1a-DIO-eYFP was injected into the left dorsal hilus. The long-range axons of MCs are illustrated schematically with green dashes in the left hippocampus. Contralateral projections (right hippocampus; grey) are addressed in Figure 2. (c) Representative viral expression of MCs and their axons (GFP) across the septotemporal DG in a female *Crlr-Cre<sup>+/-</sup>* mouse. Hoechst counterstain (blue) was used to show the DG cell layer. (c1–c4) In the dorsal hippocampus, GFP+ expression was primarily restricted to the hilus and the inner molecular layer (IML). (c5–c8) In progressively more caudal sections, fewer hilar GFP+ cells were observed, but the width of GFP+ axons in the molecular layer increased. (c9–c10) In the most caudal sections, we evaluated, the GFP+ axons terminated in the middle molecular layer in the ventral locations (insets, arrows). GCL, granule cell layer; HIL, hilus; ML, molecular layer [Color figure can be viewed at [wileyonlinelibrary.com](http://wileyonlinelibrary.com)]

single injection into the left dorsal hilus (Figure 1b). In sections proximal to the injection site (Figure 1c1–c4), viral expression was observed strongly in the hilus and a weaker fluorescent signal was observed in the IML. Consistent with previous reports (Bernstein et al., 2020; Botterill et al., 2019), hilar GFP+ cell bodies near the injection site strongly colocalized with the glutamatergic marker *Glur2/3* (Figure S2). GFP+ axons in dorsal DG were primarily restricted to the IML (Figure 1c1–c3). As sections progressed to more

caudal regions of the hippocampus, the number of GFP+ cell bodies decreased significantly. However, the GFP+ axon became much wider and spread beyond the IML in relatively caudal sections (Figure 1c5–c8). The number of GFP+ cell bodies in the more caudal hippocampal sections we evaluated was minimal (Figure 1c9,c10). However, the pattern of axonal expression in the ML differed between the dorsal and ventral portions of these sections. Specifically, the more dorsal areas showed a wider GFP+ axon that appeared to localize to the IML

**TABLE 2** Quantification of MC axons

Dorsal injection		Inner GFP (% of ML)				Outer GFP (% of ML)				Total width (% of ML)				
D/V	Hemisphere	Upper	Lower	Crest	Lower	Upper	Crest	Lower	Upper	Crest	Lower	Upper	Crest	Lower
Dorsal sections	Ipsilateral	7.02 ± 1.09%	3.46 ± 0.44%	4.59 ± 0.63%	3.46 ± 0.44%	65.69 ± 1.16%	63.61 ± 1.45%	64.12 ± 1.43%	58.66 ± 0.97%	59.02 ± 1.56%	60.66 ± 1.57%	58.66 ± 0.97%	59.02 ± 1.56%	60.66 ± 1.57%
	Contralateral	7.65 ± 0.95%	2.91 ± 0.57%	6.53 ± 1.04%	2.91 ± 0.57%	64.71 ± 1.22%	64.32 ± 0.99%	64.08 ± 1.23%	57.06 ± 1.04%	57.78 ± 0.92%	61.34 ± 1.60%	57.06 ± 1.04%	57.78 ± 0.92%	61.34 ± 1.60%
Ventral sections	Ipsilateral	41.17 ± 2.28%	37.44 ± 1.53%	37.00 ± 1.66%	37.44 ± 1.53%	68.04 ± 1.78%	59.35 ± 2.10%	61.11 ± 1.87%	26.87 ± 1.64%	22.35 ± 1.31%	23.67 ± 1.46%	26.87 ± 1.64%	22.35 ± 1.31%	23.67 ± 1.46%
	Contralateral	38.74 ± 1.15%	34.73 ± 2.10%	38.10 ± 0.87%	34.73 ± 2.10%	65.12 ± 0.84%	61.69 ± 1.13%	62.88 ± 1.62%	26.39 ± 1.24%	23.41 ± 1.27%	27.86 ± 2.12%	26.39 ± 1.24%	23.41 ± 1.27%	27.86 ± 2.12%
Ventral injection		Inner GFP (% of ML)				Outer GFP (% of ML)				Total width (% of ML)				
D/V	Hemisphere	Upper	Lower	Crest	Lower	Upper	Crest	Lower	Upper	Crest	Lower	Upper	Crest	Lower
Dorsal sections	Ipsilateral	1.12 ± 0.39%	0.81 ± 0.32%	0.74 ± 0.25%	0.81 ± 0.32%	22.69 ± 0.95%	25.28 ± 0.84%	21.37 ± 1.10%	21.40 ± 1.04%	24.29 ± 1.00%	20.41 ± 0.96%	21.40 ± 1.04%	24.29 ± 1.00%	20.41 ± 0.96%
	Contralateral	1.83 ± 0.41%	0.37 ± 0.13%	0.44 ± 0.07%	0.37 ± 0.13%	23.33 ± 0.72%	23.94 ± 0.77%	21.27 ± 1.01%	21.40 ± 0.64%	23.20 ± 0.77%	20.54 ± 0.97%	21.40 ± 0.64%	23.20 ± 0.77%	20.54 ± 0.97%
Ventral sections	Ipsilateral	0.61 ± 0.19%	0.31 ± 0.02%	0.47 ± 0.17%	0.31 ± 0.02%	25.44 ± 0.79%	23.96 ± 0.60%	25.55 ± 1.40%	24.64 ± 0.84%	23.21 ± 0.57%	24.96 ± 1.38%	24.64 ± 0.84%	23.21 ± 0.57%	24.96 ± 1.38%
	Contralateral	2.17 ± 0.47%	0.49 ± 0.12%	0.66 ± 0.17%	0.49 ± 0.12%	23.91 ± 0.78%	23.31 ± 0.65%	22.59 ± 0.86%	21.65 ± 0.53%	22.45 ± 0.63%	21.94 ± 0.88%	21.65 ± 0.53%	22.45 ± 0.63%	21.94 ± 0.88%

Note: Quantification of the GFP+ axon in mice that were injected in the (1) dorsal or (2) ventral DG with AAV-EF1A-DIO-eYFP. Values are presented as a percent of the total molecular layer (ML) width in the upper, crest, or lower blade of the DG. For each analysis, the measurements are separated by dorsal versus ventral location of the sections that were used, and the injected (ipsilateral) versus the noninjected (contralateral) hemisphere. D/V, dorsal/ventral.

and MML. In contrast, the relatively ventral portions of the same sections showed a GFP+ axon that was primarily located in the MML (Figure 1C<sub>9b</sub>,C<sub>10b</sub>).

### 3.1.2 | Horizontal sections

As mentioned in Section 2, the hemisphere contralateral to the viral injection was sectioned horizontally. This allowed better evaluation of ventral hippocampus and also was used to examine the contralateral projection of MCs (Figures 2a,b and S3). In contrast to past reports that the MC axon targets the contralateral DG in a homotopic fashion, we found that GFP+ axons were observed throughout the dorsal-ventral axis in the noninjected hemisphere. This finding suggests that commissurally projecting MC axons are heterotopic and not homotopic as previously thought (Myers & Scharfman, 2009; Scharfman & Myers, 2012). In dorsal horizontal sections, GFP+ axons were observed throughout the ML (Figure 2c1,c2). As sections progressed from dorsal to more ventral hippocampus the GFP+ axon became increasingly further away from the GCL border (Figure 2c3,c4). In the most ventral sections that were evaluated, the GFP+ axon was primarily in the MML with some labeling in the OML and almost no expression in the IML (Figure 2c5,c6). Interestingly, scattered GFP+ hilar cells were observed throughout the dorsal-ventral axis of the contralateral (noninjected) DG (Figure 2c1-c6) although they were relatively rare compared to the dense labeling of somata at the injection site. High-resolution Z-stacks of the contralateral cells showed that they had morphology consistent with MCs, such as a large multipolar soma, numerous spiny dendrites, and dendritic regions with clusters of spines (Figure S3). These contralateral cells may be a result of anterograde or retrograde labeling, which has been reported for multiple AAV serotypes, including AAV5 (Haery et al., 2019).

## 3.2 | GFP+ expression following a single ventral hilus injection

### 3.2.1 | Coronal sections

In a separate set of experiments, mice received a single viral injection into the left ventral hilus (Figure 3a). Similar to the dorsal injection, a single ventral injection also resulted in GFP+ axon labeling throughout the entire septotemporal extent of the DG (Figure 3b). In dorsal sections, that is, distal to the injection site, there were no GFP+ cells within the hilus (Figure 3b1-b4). As sections progressed to more caudal and ventral regions, the number of GFP+ hilar cells increased significantly (Figure 3b5-b10). A very small number of weakly-labeled GFP+ cells were observed in the CA3c region of some sections (Figure 3b7-b9), consistent with previous reports (Fredes et al., 2020; Yeh et al., 2018). Importantly, the GFP+ axon was largely restricted to the IML of the DG throughout the entire septotemporal axis of the DG. This result suggests that dorsal and ventral MCs have distinct axonal projections.



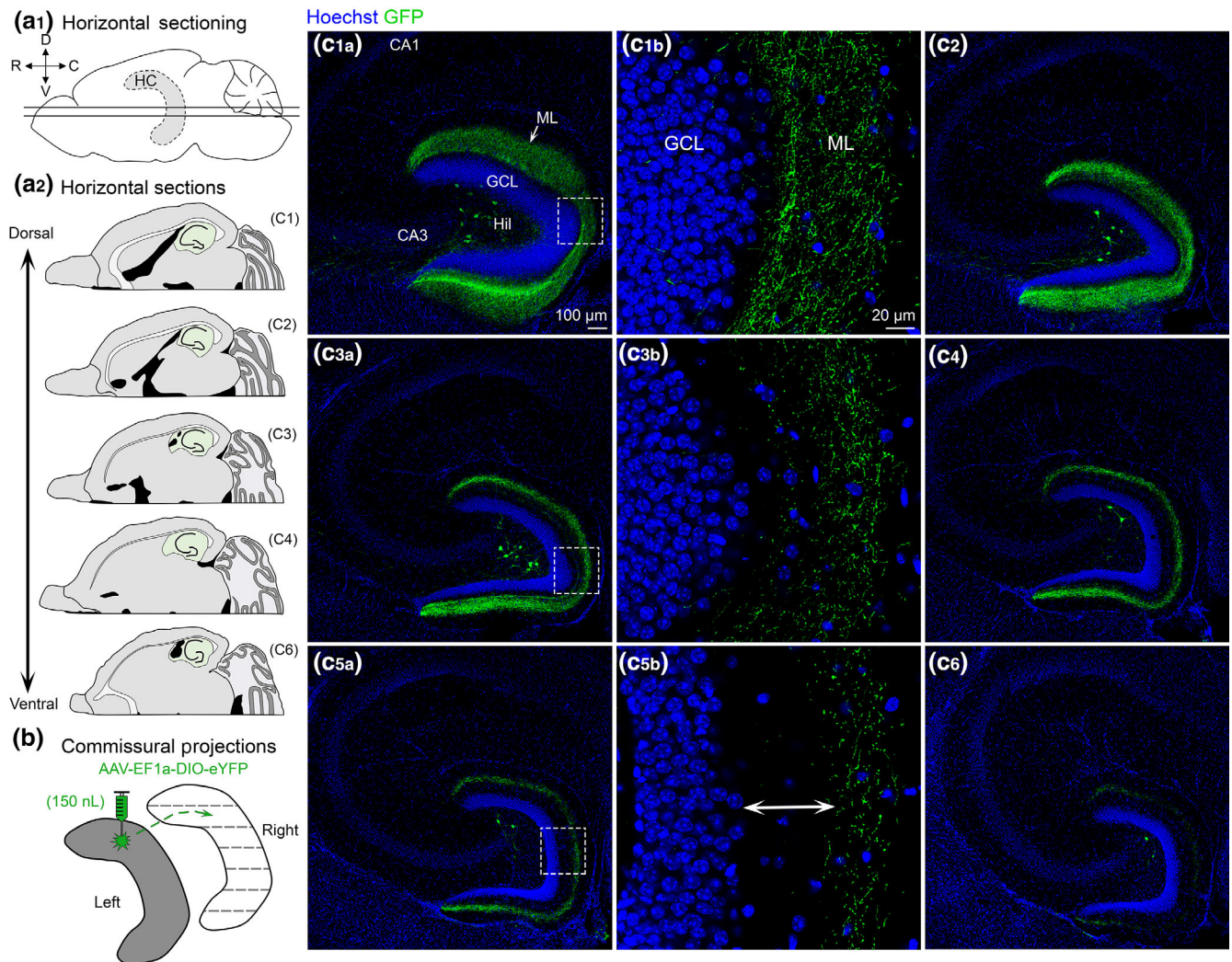


**FIGURE 2** Contralateral projections of dorsal MC axons across the septotemporal axis of the DG. (a1) Side view of the brain showing the septotemporal extent of the hippocampus (HC; grey with dashed border). Straight horizontal lines are shown to illustrate the horizontal plane. (D) Dorsal; (V) Ventral; (R) Rostral; (C) Caudal. (a2) Representative schematic of horizontal sections from a dorsal level to a progressively more ventral level (green). (b) To evaluate contralateral projections of dorsal MCs, the left hilus (grey) was injected and the right hippocampus (white) was evaluated in the horizontal plane. (c) Representative viral expression in a female *Crlr-Cre<sup>+/-</sup>* mouse. Viral expression in the contralateral hemisphere is shown from sections that were dorsal and progressively more ventral. (c1–c2) In the relatively dorsal sections, there were GFP+ axons throughout the molecular layer. (c3–c4) “Mid” sections (between the dorsal sections in c1–c2 and the ventral sections in c5–c6) showed GFP+ axons that terminated increasingly further away from the GCL border. (c5–c6) GFP+ axons in ventral sections were primarily in the MML (arrow). GCL, granule cell layer; HIL, hilus; ML, molecular layer [Color figure can be viewed at [wileyonlinelibrary.com](http://wileyonlinelibrary.com)]

### 3.2.2 | Horizontal sections

To best evaluate the commissural projections of ventral MCs throughout the dorsal–ventral axis, brains were hemisected and the right (noninjected) hemisphere was cut in the horizontal plane (Figure 4a). Similar to dorsal hilar injections, mice with a ventral hilar injection showed GFP+ axon expression throughout the entire dorsal–ventral axis of the contralateral DG (Figure 4b). This observation provides further support for the notion that contralateral MC axons are heterotopic and not homotopic (as discussed above). Furthermore, similar to the coronal sections, the GFP+ axon was restricted primarily to the

IML throughout the entire dorsal–ventral axis (Figure 4b<sub>1b</sub>, b<sub>3b</sub>, b<sub>5b</sub>). Interestingly, unlike dorsal injections, mice injected in the ventral hilus had few or no GFP+ cells in the hilus of the contralateral DG.

### 3.3 | Measurements of the GFP+ axon in dorsal and ventral injected mice

Next, we sought to quantify the previously described differences in GFP+ axonal expression following a single dorsal ( $n = 8$ ) or ventral ( $n = 8$ ) hilar injection.

### 3.3.1 | GFP+ axon measurements for dorsal viral injections

Following a single dorsal viral injection (Figure 5a), we evaluated the GFP+ axons in dorsal and ventral sections (Figure 5b1,b2). Using the criteria described in Methods and shown in Figure 5b3, we first measured the distance from the GCL/IML border to the start of the band of GFP+ immunofluorescence in the ML (Figure 5c). The values are reported as a percentage of the total ML width (Section 2). A two-way ANOVA revealed a significant main effect of septotemporal location ( $F[1,42] = 1,532.0, p < .001$ ), attributable to the GFP+ signal being closer to the GCL/IML border in dorsal sections ( $5.37 \pm 0.45\%$ ) than ventral sections ( $37.56 \pm 0.79\%$ ). Based on the division of the ML into sublayers that are equaled to thirds of the ML (33.33, 66.67, 100%), the results indicate that the GFP+ signal always began in the IML of dorsal sections but began in the MML of ventral sections.

We also observed a main effect of blade ( $F[2, 42] = 7.47, p < .002$ ). In dorsal sections, the distance between the GCL/IML

border and GFP+ signal was significantly greater in the upper blade ( $7.19 \pm 0.57\%$ ) compared to the lower blade ( $3.11 \pm 0.31\%$ ;  $p = .018$ ). A similar finding was observed in ventral sections, where the distance between the GCL/IML border and GFP+ signal was significantly greater in the upper blade ( $39.44 \pm 1.22\%$ ) compared to the lower blade ( $35.76 \pm 1.78\%$ ;  $p = .035$ ).

Next, we measured the distance from the GCL/IML border to the point where the GFP+ terminal plexus ended in the ML (Figure 5d). A two-way ANOVA revealed a significant main effect of blade ( $F[2,42] = 3.40, p = .043$ ), with Tukey's post hoc test showing that the distance to the outer GFP+ fluorescence was greater in the upper blade of ventral sections ( $66.08 \pm 1.07\%$ ) compared to the crest ( $60.88 \pm 1.29\%$ ;  $p = .007$ ). No other blade differences were observed (all  $p$  values  $>.071$ ). The two-way ANOVA also found that there was no effect of septotemporal location ( $F[1,42] = 1.41, p = .242$ ). However, this finding is still notable because these measurements show that the dorsal ( $64.23 \pm 0.59\%$ ) and ventral sections ( $63.12 \pm 0.82\%$ ) projected almost to the MML/OML border (i.e., 66.67% of the ML).

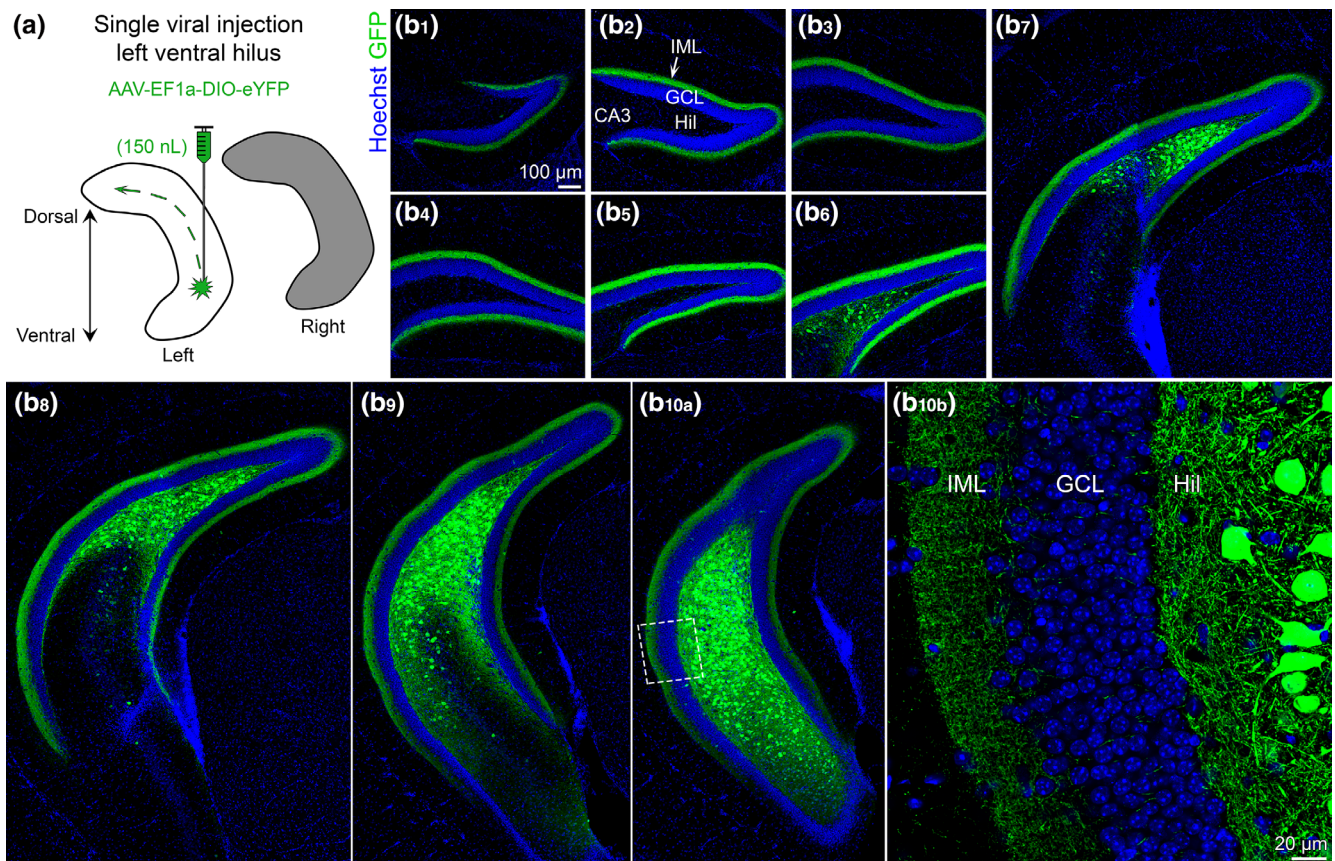


**FIGURE 3** Viral expression in ventral MCs and their axons across the septotemporal axis of the DG. (a) Viral injection schematic. AAV-EF1a-DIO-eYFP was injected into the left ventral hilus. The long-range axons of ventral MCs are depicted with the green dashes in the left hippocampus (white). Contralateral projections of ventral MCs (right hippocampus; grey) are addressed in Figure 4. (b) Representative viral expression of ventral MCs and their axons (GFP+) across the septotemporal DG in a female *Drd2-Cre<sup>+/-</sup>* mouse. Hoechst counterstain (blue) was used to show the DG cell layer. (b1–b5) In the dorsal hippocampus, GFP+ expression was primarily restricted to the inner molecular layer (IML). (b6–b8) In sections that were progressively more caudal, GFP+ expression was observed in the hilus and IML in the part of the DG that was more ventral. (b9–b10) In sections that show the ventral DG, GFP+ expression was observed in the hilus and IML. GCL, granule cell layer; HIL, hilus; IML, inner molecular layer [Color figure can be viewed at [wileyonlinelibrary.com](http://wileyonlinelibrary.com)]



There probably were some axons that entered the OML because a few mice had “outer” GFP+ scores between 67 and 69% (Figure 5d, indicating that the furthest GFP+ projections could be detected as far as the OML but this was generally rare (consistent with Buckmaster et al., 1996).

We also measured the total width of the GFP+ terminal plexus in the ML (Figure 5e). A two-way ANOVA revealed a significant main effect of septotemporal location ( $F[1,42] = 1,618.0, p < .001$ ), with dorsal sections ( $58.89 \pm 0.63\%$ ) having a significantly wider GFP+ axon than the ventral sections ( $25.47 \pm 0.66\%$ ). The results also revealed a main effect of blade ( $F[2,42] = 3.98, p = .026$ ). However, Tukey's post hoc test found no significant differences between blades (all  $p$  values  $>.055$ ). Given our previous inner and outer GFP+ measurements, these findings collectively indicate that the dorsal GFP+ axon began in the IML and extended throughout the MML, whereas

the ventral GFP+ axon began in the MML and terminated primarily in the MML.

### 3.3.2 | GFP+ axon measurements following a ventral viral injection

Using the same approach as above, we quantified sections from mice injected in the ventral hilus (Figure 5f–g). First, we measured the distance between the GCL border and the nearest GFP+ terminal plexus in the ML. A two-way ANOVA revealed a significant main effect of blade ( $F[2,42] = 12.91, p < .001$ ) but no difference between septotemporal locations ( $F[1,42] = 0.278, p = .601$ ; Figure 5h). Within dorsal sections, the distance was significantly greater in the upper blade ( $1.53 \pm 0.26\%$ ) compared to the crest ( $0.59 \pm 0.13\%$ ) and lower

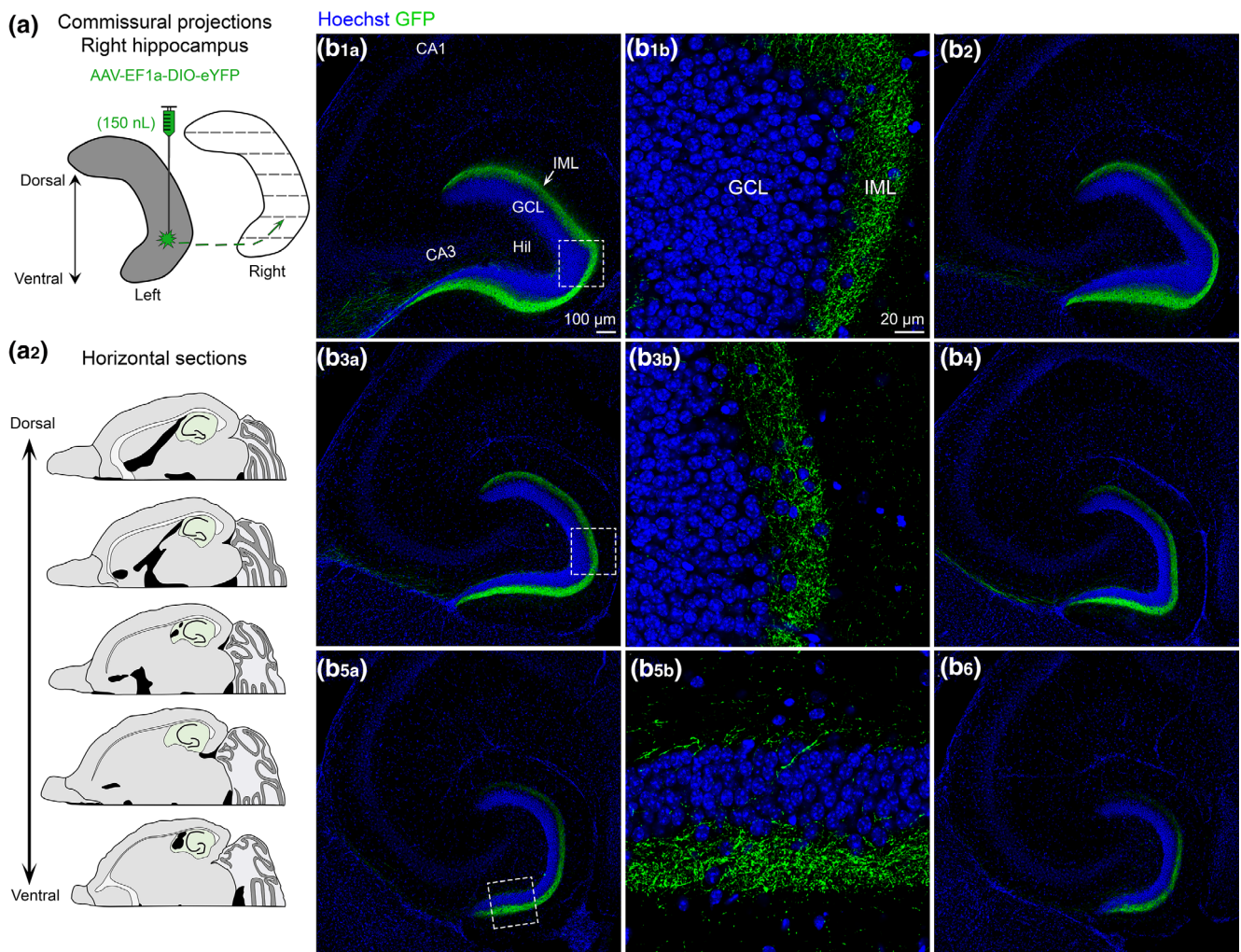


**FIGURE 4** Contralateral projections of ventral MC axons across the septotemporal axis of the DG. (a1) To evaluate contralateral projections of ventral MCs, the left hilus was injected with AAV-EF1a-DIO-eYFP (grey) and the right hippocampus (white) was evaluated in the horizontal plane. (a2) Representative schematic of horizontal sections from dorsal to more ventral hippocampus (green). (b) A representative example of contralateral GFP+ expression in a female *Drd2-Cre<sup>+/-</sup>* mouse. Sections begin at dorsal levels and progress toward more ventral locations. (b1–b6) The contralateral projections of ventral MCs appear to be primarily restricted to the IML across all sections. HIL, hilus; GCL, granule cell layer; IML, inner molecular layer [Color figure can be viewed at [wileyonlinelibrary.com](http://wileyonlinelibrary.com)]



blade ( $0.58 \pm 0.19\%$ ; all  $p$  values  $<.009$ ). Similarly, within ventral sections, the distance was significantly greater in the upper blade ( $1.42 \pm 0.32\%$ ) compared to the crest ( $0.60 \pm 0.21\%$ ) and lower blade ( $0.41$

$\pm 0.09\%$ ; all  $p$  values  $<.024$ ). Taken together, these results indicate that a ventral hilus injection resulted in a GFP+ axon plexus that did not extend beyond the IML the in dorsal and ventral sections.

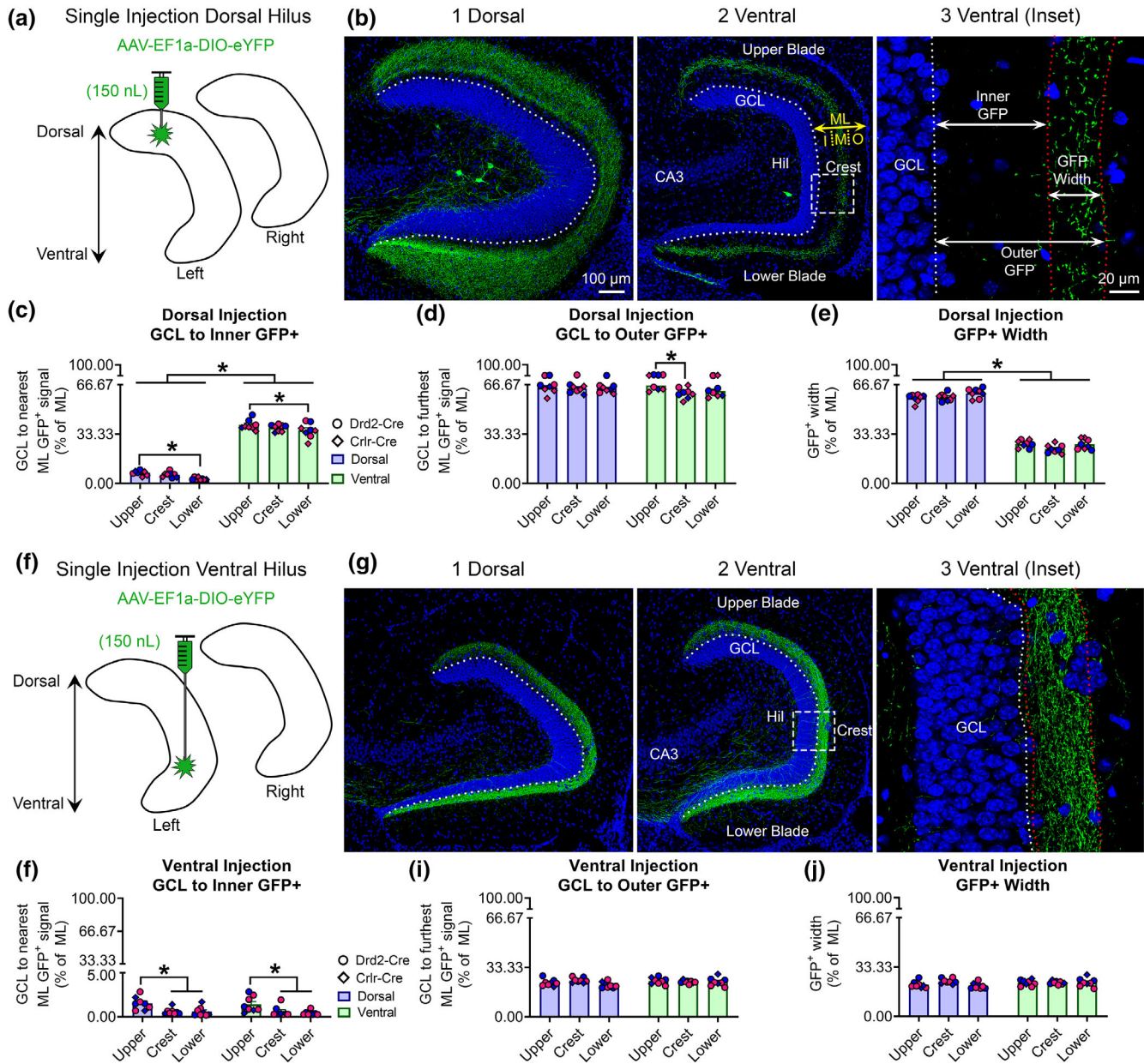


**FIGURE 5** Quantitative analysis of the GFP+ MC axon terminal plexus. (a) Schematic showing that AAV-EF1a-DIO-eYFP was injected into the left dorsal hilus. (b1–b2) A representative example of contralateral GFP+ axon terminals in the (b1) dorsal and (b2) ventral DG of a female Crlr-Cre+/- mouse. The width of the molecular layer (ML) is depicted by the yellow arrow and the approximate subdivisions of the inner (I), middle (M), and outer (O) are separated by dashes. (b3) A schematic shows the inner, outer, and width measurements for the GFP+ axon plexus. Measurements were made in the center of the upper blade, crest, and center of the lower blade and reported as a % of total ML width. (c) In dorsally injected mice, the GFP+ axon was near the GCL/IML border in dorsal sections, but primarily in the MML of ventral sections. Blue and pink data points represent male and female mice, respectively. (d) The outermost distance of the GFP+ axon was approximately 63–64% of dorsal and ventral sections, indicating the GFP+ axons primarily terminated in the MML. (e) The total width of the GFP+ axon was significantly greater in dorsal than ventral sections. (f) A schematic for additional animals where AAV-EF1a-DIO-eYFP was injected into the left ventral hilus. (g1–g2) A representative example of contralateral GFP+ axons in the relatively (g1) dorsal and (g2) ventral DG of a male Drd2-Cre+/- mouse. (g3) A schematic showing GFP+ axon measurements. (h) The inner distance did not differ between dorsal and ventral sections, but the parts of the DG differed. (i,j) The outer GFP+ distance and total GFP+ width did not differ between dorsal and ventral sections. Notably, all measurements from ventrally injected mice were below 33%, indicating the axon was restricted to the IML. \* $p < .05$  [Color figure can be viewed at wileyonlinelibrary.com]

Next, we evaluated the furthest distance of GFP+ immunofluorescence in the ML. A two-way ANOVA revealed no effect of septotemporal location ( $F[1,42] = 1.53, p = .223$ ) or blade ( $F[2,42] = 2.304, p = .112$ ; Figure 5i). The furthest GFP+ immunofluorescent signal in the ML was  $23.02 \pm 0.47\%$  for dorsal sections and  $23.76 \pm 0.42\%$  for ventral sections. We also measured the total width of the GFP+ immunofluorescence in the ML of mice that were injected in the ventral hilus (Figure 5j). A two-way ANOVA found no effect of septotemporal location ( $F[1,42] = 2.06, p = .159$ ) or blade ( $F[2,42] = 2.221, p = .122$ ) on total GFP+ width. Notably, the average width of the GFP+ axon in the ML was  $21.89 \pm 0.48\%$  of the ML for dorsal sections and  $22.76 \pm 0.42\%$  for ventral sections. Taken together, these findings indicate that the start and end of the GFP+ axon in ventral injected mice was primarily restricted to the inner two-thirds of the IML (i.e., ~22%). This observation is in stark contrast to the dorsal injected mice that had projections that began in the IML or MML and extended toward the MML/OML border.

### 3.4 | Comparisons between mice that were injected dorsally or ventrally

Next, we compared measurements of the ML axon across the septotemporal axis between dorsally and ventrally injected mice (Figure S4). We used the measurements from mice that were injected dorsally and ventrally above, but averaged the upper, crest, and lower blade measurements for one comprehensive measurement. A two-way ANOVA found a main effect of injection site ( $F[1,28] = 1.558, p < .001$ ), septotemporal location ( $F[2,28] = 944.3, p < .001$ ), and a significant interaction ( $F[1,28] = 955, p < .001$ ) for measurements of the inner GFP+ distance. Tukey's post hoc test found that dorsal and ventral sections of dorsally injected mice had a significantly greater inner GFP+ distance than the dorsal and ventral sections of ventrally injected mice (all  $p$  values  $< .001$ ; Figure S4a). Next, we evaluated the outer GFP+ distance in the ML and a two-way ANOVA revealed a significant main effect of injection site ( $F[1,28] = 4.312, p < .001$ ), but no difference across the septotemporal axis ( $F[1,28] = 0.09, p = .764$ ). Tukey's post hoc test revealed that the GFP+ axon in dorsally injected mice terminated further in the ML than ventrally injected mice across dorsal and ventral sections (all  $p$  values  $< .001$ ; Figure S4b). We also evaluated the total width of the GFP+ axon in dorsally and ventrally injected mice across the septotemporal DG. A two-way ANOVA found a significant main effect of injection site ( $F[1,28] = 1.264, p < .001$ ), septotemporal location ( $F[1,28] = 850, p < .001$ ), and a significant interaction ( $F[1,28] = 942.7, p < .001$ ). Tukey's post hoc test found that width of the GFP+ axon was significantly greater in dorsally injected mice compared to ventrally injected mice throughout the dorsal-ventral axis (all  $p$  values  $< .011$ ; Figure S4c).

To further demonstrate differences in the axons of dorsal and ventral MCs, *Drd2-Cre<sup>+/-</sup>* mice ( $n = 3$ ) underwent dual injections where AAV-EF1a-DIO-mCherry was injected into the dorsal hilus and AAV-EF1a-DIO-eYFP was injected into the ventral hilus (Figure S4d).

Similar to the quantification described in Figure S4a–c, dorsal MCs (expressing mCherry) had a wider axon plexus in dorsal sections than ventral sections (where MCs were labeled by eYFP). In addition, the eYFP+ axon plexus of ventral MCs terminated primarily in the IML in dorsal sections but the mCherry-expressing axons of dorsal MCs terminated primarily in the MML of ventral sections.

### 3.5 | CaMKIIa injections in the hilus result in a similar axonal pattern of expression in the ML as MC-specific targeting

Next, we used a different approach than *Drd2* or *Crlr-Cre* mice because of the possibility that these mouse lines express virus in hilar GABAergic neurons. To this end, we targeted excitatory neurons in the DG using a viral construct that utilized the calcium/calmodulin-dependent protein kinase II (CaMKIIa) promoter. A virus tagged with mCherry was used instead of GFP simply due to availability of viruses. This approach also labels excitatory cells like the GCs and CA3c pyramidal neurons, but this was actually useful as explained below.

#### 3.5.1 | CaMKIIa-mCherry injection into the dorsal hilus

The dorsal hilus was injected with AAV-CaMKIIa-ChR2(H134R)-mCherry using identical parameters as the Cre-dependent expression experiments (Figure 6a). *Drd2-Cre<sup>-/-</sup>* mice ( $n = 3$ ) were used since the *Cre<sup>+/-</sup>* mice were not needed for viral expression and not valuable in these experiments, as explained above. Brains were sectioned in the horizontal plane. In sections near the injection site, mCherry+ viral expression was observed in GCs, mossy fibers, hilar cells (putative MCs), and CA3 pyramidal neurons (Figure 6b1,b2), consistent with the selectivity of CaMKIIa for excitatory neurons. As sections were evaluated in more ventral regions, mCherry+ expression in the ML became increasingly further from the GCL, consistent with the pattern observed when MCs were targeted selectively (Figure 6b3–b7). In addition, mCherry+ expression was also observed in the CA3 stratum radiatum of all sections, presumably due to targeting of the Schaffer collateral axons of CA3 pyramidal neurons.

Commissural projections were also assessed by evaluating the noninjected hemisphere of the same mice (Figure 6c). Consistent with our previous experiments, a similar pattern of mCherry+ expression was observed across the dorsal-ventral axis, whereby mCherry+ expression was seen throughout the ML in dorsal sections (e.g., Figure 6d1) and appeared restricted to the MML of ventral sections (e.g., Figure 6d4–d6). Notably, we did not observe mCherry+ somata in the contralateral hilus like the AAV-DIO-eYFP experiments. The fact that we observed a similar pattern of mCherry+ expression in the ML without labeling contralateral somata suggests that the small number of contralateral somata in YFP experiments did not influence staining in the ML. Interestingly, contralateral mCherry+ expression was also observed in the CA3 stratum radiatum of dorsal sections



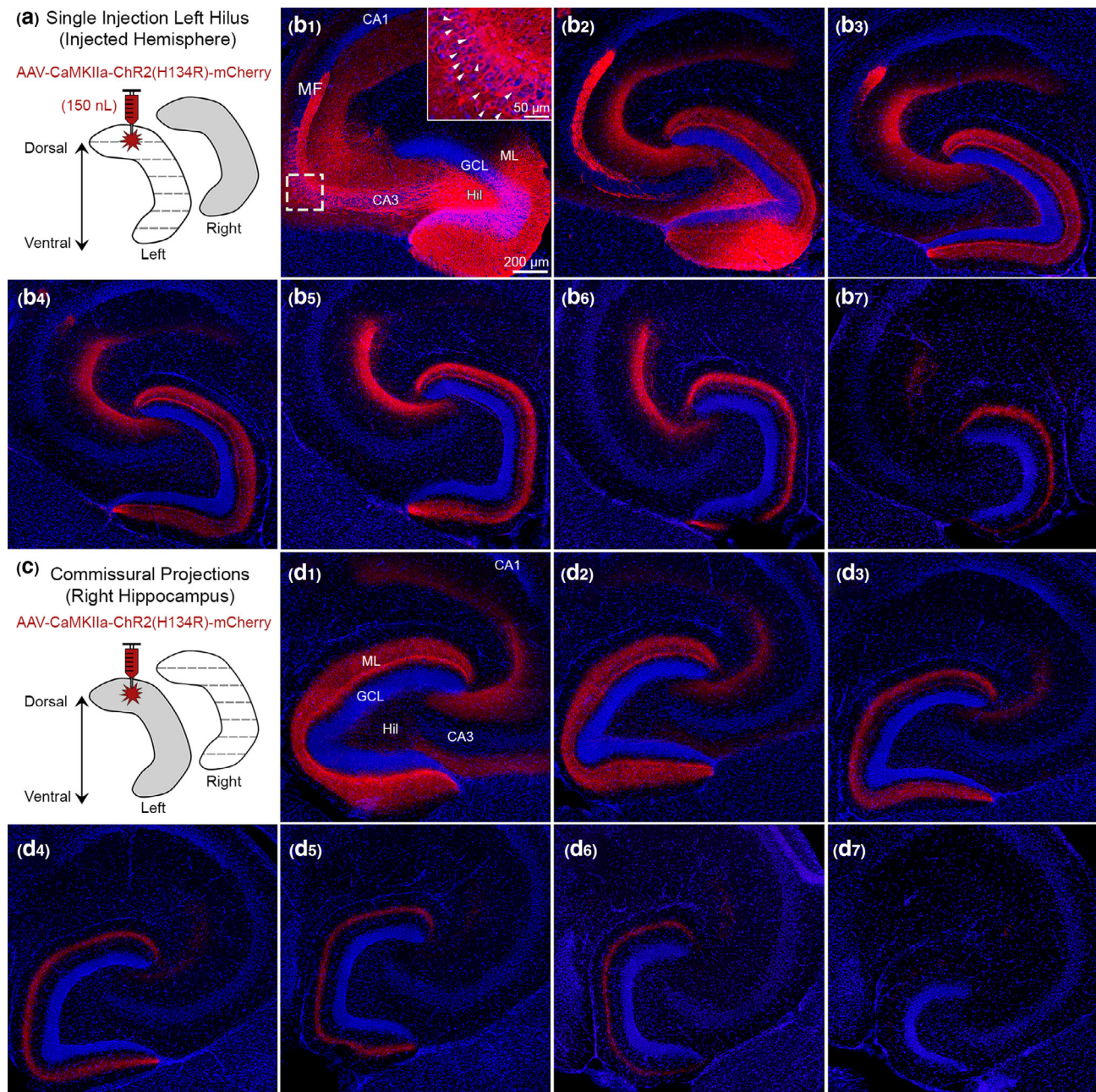


**FIGURE 6** Use of CaMKIIa to probe the specificity of GFP for MCs. (a) Viral injection schematic. A total of 150 nl of AAV-CaMKIIa-ChR2 (H134R)-mCherry was injected into the left dorsal hilus to target excitatory neurons. (b1–b2) Near the injection site, viral expression was observed in GCs, MCs, and CA3 pyramidal neurons (inset; white arrowheads). Granule cell mossy fibers (MF) axons were also labeled where they normally project, CA3 stratum lucidum. (b3–b7) Long-range mCherry+ axons showed a similar pattern of viral expression in the molecular layer as Drd2-Cre or Crlr-Cre mice injected in the dorsal DG with a virus to express GFP. (c) Contralateral axons were evaluated in the right hippocampus. (d1–d7) Contralateral mCherry+ axons showed a similar pattern in the molecular layer as Drd2-Cre and Crlr-Cre injected with a virus expressing GFP in the dorsal hilus. This figure shows that injection of AAV to express CaMKIIa in the dorsal hilus results in a similar pattern of axon labeling as an injection of AAV to express GFP in MCs. Representative images are from a female Drd2-Cre<sup>-/-</sup> mouse. GCL, granule cell layer; HIL, hilus; ML, molecular layer [Color figure can be viewed at [wileyonlinelibrary.com](http://wileyonlinelibrary.com)]

(Figure 6d1–d3), which was not seen in experiments targeting the MCs only.

Taken together, mCherry+ expression in the ipsilateral and contralateral ML was similar to MC-specific experiments that targeted the dorsal hilus. These results support the notion that the dorsal–ventral

distribution of GFP+ axons described in previous experiments are attributable to MCs rather than nonspecific targeting of GABAergic hilar cell populations. They also support the idea that GCs and pyramidal neurons of CA3 did not contribute significantly to data using GFP in Drd2-Cre or Crlr-Cre mice, and the role of CA3 is addressed further below.



### 3.5.2 | CaMKIIa-mCherry injection into the dorsal CA3 region

Given the observation that CA3 neurons can be labeled in *Drd2-Cre* or *Crlr-Cre* lines, we targeted the CA3 area with virus to determine whether viral expression in CA3 can contribute to viral expression in the ML. *Drd2-Cre<sup>-/-</sup>* ( $n = 3$ ) mice were injected in the dorsal CA3 (a/b subfield) with AAV-CaMKIIa-ChR2(H134R)-mCherry (Figure S5a). Pilot experiments found that larger volumes or injections more proximal to CA3c labeled MCs and therefore prevented us from determining whether CA3 could contribute to ML immunofluorescence. In sections near the injection site, we observed viral expression in the CA3 pyramidal cell layer (Figure S5b1–b3). We also observed a band of mCherry+ expression in CA3 stratum radiatum, supporting the

notion that CA3 pyramidal neurons caused the stratum radiatum mCherry+ expression in the CaMKIIa experiments that targeted the hilus (Figure 6). Importantly, throughout the dorsal-ventral axis, there was no mCherry+ immunofluorescence in the ML.

To more directly address a contribution of CA3c axons to the MML labeling, *Crlr-Cre<sup>+/-</sup>* mice ( $n = 2$ ) were injected in the ventral hilus with AAV-EF1a-DIO-eYFP (Figure S5c). Consistent with previous reports (Bernstein et al., 2020; Jinde et al., 2012), we observed GFP in hilar cells and in CA3c pyramidal neurons (Figure S5d). Notably, the ML axon was primarily restricted to the IML, consistent with what we observed in *Drd2-Cre* mice that received ventral injections without significant CA3 contamination. Taken together, these results suggest that viral expression in CA3 subfields did not contribute to viral expression in the MML.

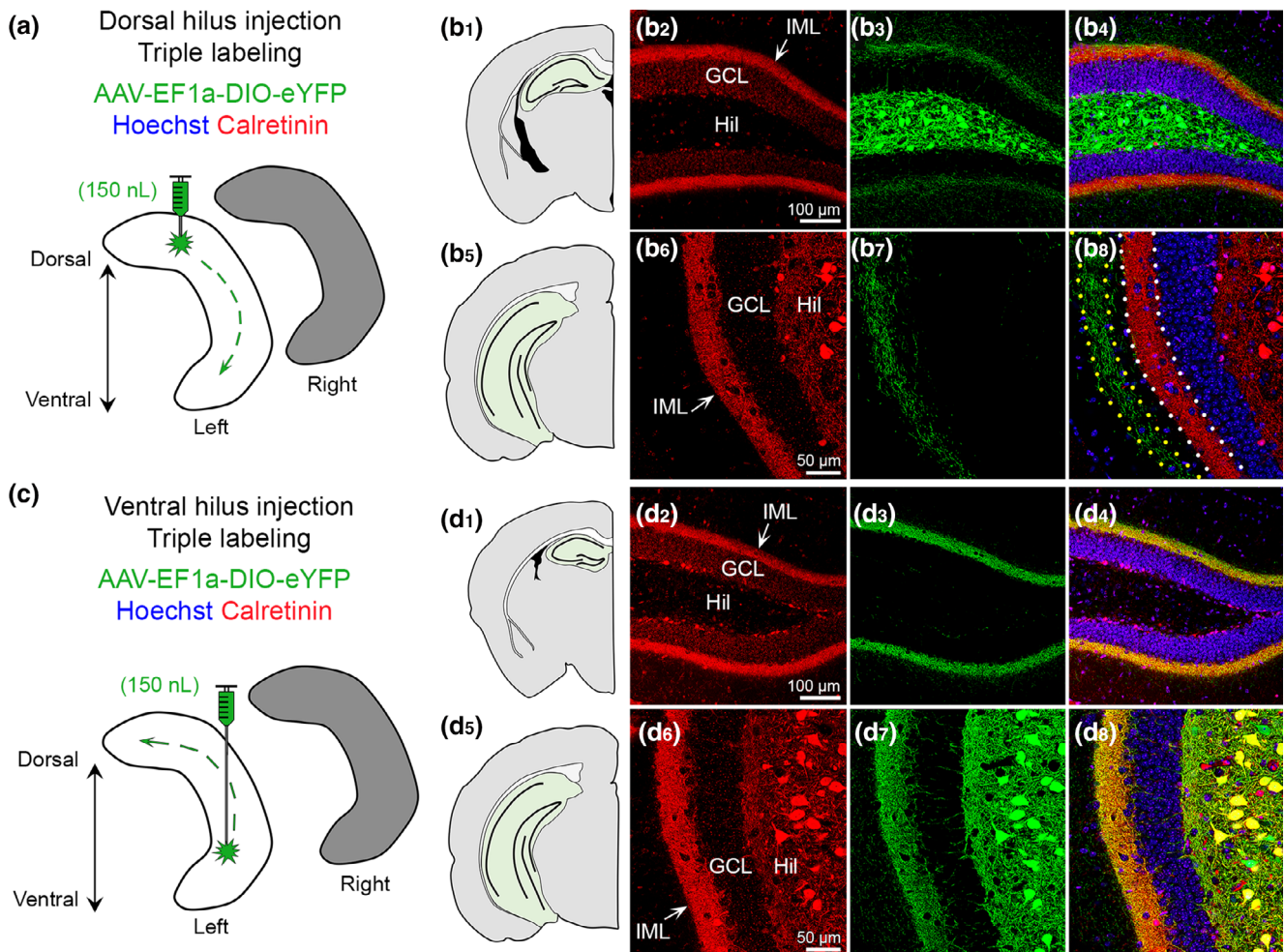


**FIGURE 7** Calretinin labels ventral but not dorsal MCs. (a) Viral injection schematic. AAV-EF1a-DIO-eYFP was injected into the left dorsal hilus. (b1–b4) In the dorsal DG, calretinin (red) is primarily in the IML of the DG, whereas viral expression (green) is strong in hilar cells and weak in the IML. (b5–b8) In ventral hippocampus, calretinin expression (red) is in putative hilar MCs and the IML. Long-range GFP+ axons are observed in the molecular layer adjacent to calretinin immunofluorescence in the IML (dotted borders). Representative images are from a female *Crlr-Cre* +/- mouse. (c) Viral injection schematic. AAV-EF1a-DIO-eYFP was injected into the left ventral hilus. (d1–d4) Calretinin (red) and GFP+ long-range axons are primarily in the IML and appear to colocalize (yellow). (d5–d8) In ventral sections, calretinin (red) and GFP strongly overlap within hilar cell bodies and the IML (yellow). Representative images are from a female *Drd2-Cre* +/- mouse. GCL, granule cell layer; HIL, hilus; IML, inner molecular layer [Color figure can be viewed at [wileyonlinelibrary.com](http://wileyonlinelibrary.com)]

### 3.6 | Ventral but not dorsal MCs correspond to calretinin immunoreactivity

In the mouse, calretinin is widely used as a marker for MC somata and MC axons in the IML. Consistent with past reports (Blasco-Ibanez & Freund, 1997; Fujise, Liu, Hori, & Kosaka, 1998), calretinin expression of MC somata is primarily observed in the ventral hilus but not dorsal hilus (Figure S6). However, calretinin immunoreactivity in the IML is observed throughout the entire septotemporal axis of the DG (Blasco-Ibanez & Freund, 1997; Fujise et al., 1998). This led us to hypothesize that calretinin IML immunoreactivity is due to ventral but not dorsal MCs.

First, we evaluated mice injected in the dorsal hilus with AAV-EF1a-DIO-eYFP and sections were processed for calretinin immunofluorescence ( $n = 6$ ; Figure 7a). In dorsal sections (Figure 7b1), we found that calretinin immunofluorescence was observed in the IML; however, cell bodies in the hilus were not labeled with calretinin. In contrast, GFP+ expression was strongly expressed in hilar cells and moderately expressed in the IML, resulting in minimal colocalization of calretinin and GFP (Figure 7b2–b4). In ventral sections, calretinin immunofluorescence was observed in hilar cells and the IML (Figure 7b5,b6). Remarkably, GFP+ axons terminated in the MML–OML, adjacent to the calretinin immunofluorescence in the IML (Figure 7b7,b8). This result is consistent with prior studies showing that dorsal MC somata lack calretinin expression. It also helps explain why the MML axons of dorsal MCs has not been reported using classic immunohistochemical approaches. Indeed, it appears that viral labeling is required to study dorsal MCs and their unique axonal plexus.

Next, we evaluated mice ( $n = 6$ ) injected in the ventral hilus with AAV-EF1a-DIO-eYFP and processed sections for calretinin immunofluorescence (Figure 7c). In dorsal sections (Figure 7d1), we found that calretinin and GFP+ immunofluorescence were primarily in the IML and showed strong colocalization (Figure 7d2–d4). In ventral sections (Figure 7d5), we found that calretinin and GFP+ immunofluorescence was similar and showed a high degree of colocalization in the IML (MC axons) and hilus (cell bodies; Figure 7d6–d8). These results suggest that ventral MCs express calretinin in their cell bodies and their axons in the IML across the dorsal–ventral axis of the DG.

### 3.7 | GFP+ axons in the ML show minimal colocalization with GABAergic markers

Next, we sought to determine whether nonspecific targeting of GABAergic neuron axons contributed to viral expression in the ML. Notably, GABAergic hilar neurons such as hilar perforant path-associated (HIPP) cells are hilar cells with axons that project locally to the hilus, MML–OML and to the contralateral MML–OML (Deller & Leranth, 1990; Eyre & Bartos, 2019). To address the potential concern that some of the GFP+ axons were due to HIPP cells, we injected mice in either the dorsal ( $n = 3$ ) or ventral ( $n = 3$ ) hilus with AAV-EF1a-DIO-eYFP and processed the tissue with two widely used

antibodies for GABAergic terminals: VGAT and GAD67. Using these two markers, we also could address the possibility that some of the axons in the IML were due to HICAP cells (Halasy & Somogyi, 1993; Han, Buhl, Lorinczi, & Somogyi, 1993), and some axons in the MML or OML were from MOPP cells (Halasy & Somogyi, 1993; Han et al., 1993) or molecular layer neurogliaform cells (Armstrong, Szabadics, Tamas, & Soltesz, 2011).

#### 3.7.1 | Vesicular GABA transporter

First, we evaluated vesicular GABA transporter (VGAT) immunofluorescence in mice injected in the left dorsal hilus with AAV-EF1a-DIO-eYFP (Figure S7a). VGAT immunofluorescent terminals were observed around GC somata and throughout the ML (Figure S7b), consistent with previous studies of GABAergic terminal distribution in the DG (Freund & Buzsaki, 1996; Houser, 2007). In both dorsal and ventral sections, the GFP+ axon in the ML failed to show clear colocalization with VGAT (Figure S7b1,b2). However, GFP+ terminals were often adjacent to or near VGAT+ puncta, which is not surprising given the density of MC and GABAergic labeling. In a few cases GFP+ and VGAT+ immunofluorescence appeared to overlap and produce a yellow product, but this was due to a GFP+ bouton on or overlapping a GABAergic bouton in a different focal plane. We also evaluated VGAT immunofluorescence in mice that received AAV-EF1a-DIO-eYFP in the left ventral hilus (Figure S7c). In mice injected in the ventral hilus, the GFP+ axons were primarily restricted to the IML (Figure S7d1,d2). Similar to the dorsally injected mice, the GFP+ axons showed minimal colocalization with VGAT in both dorsal and ventral sections. Taken together, these results suggest that the GFP+ axons in dorsally and ventrally injected mice were unlikely to be due to GABAergic terminals. This finding is further supported by the CaMKIIa experiments that targeted excitatory neurons in the dorsal hilus that produced a similar pattern of ML immunofluorescence across the dorsal–ventral axis as GFP.

#### 3.7.2 | GAD67

Next, we evaluated Glutamate Decarboxylase 67 (GAD67) immunofluorescence in mice that received a viral injection of AAV-EF1a-DIO-eYFP into the dorsal or ventral hilus (Figure S8a,c). Similar to VGAT, GAD67 was observed around GCs and throughout the ML; however, GAD67 also resulted in some somatic labeling throughout the hilus and ML (Figure S8b1,d2). In mice where the viral injection was the dorsal hilus, we observed minimal GFP+ and GAD67+ colocalization and this was true for sections that were located throughout the dorsal–ventral axis (Figure S8b1,b2). A similar observation was made for mice that received viral injections in the ventral hilus. Indeed, both dorsal and ventral sections showed minimal GFP/GAD67+ colocalization (Figure S8d1,d2). In summary, GAD67 immunofluorescence showed minimal colocalization in GFP+ axons, suggesting that the GFP+ axons are primarily gamma-aminobutyric acid (GABA)



negative. This finding is further supported by the VGAT immunofluorescence which also showed minimal colocalization with GFP+ immunofluorescent MC axons.

### 3.8 | Mistargeted viral injections do not cause ML GFP+ expression

Finally, we show that GFP+ expression is absent in the ML of animals that received viral injections that were outside of the DG. These injections were accidental and due to experimenter error such as misreading the coordinates of the stereotaxic apparatus, head tilts, or lowering the injection syringe to an inaccurate depth (or any combination of these factors). In one representative example, we found that an accidental injection in the thalamus of a *Drd2-Cre<sup>+/-</sup>* resulted in GFP+ cell expression near the injection site, but no expression was observed in the DG (Figure S9). Thus, when virus labeled areas surrounding but not within DG, we observed no viral expression in the DG. Taken together with the previous results, these data suggest that viral expression in the ML required viral expression in hilar cells and did not arise from other local sources (e.g., CA3; Figure S5) or regions outside of the DG such as the thalamus.

## 4 | DISCUSSION

### 4.1 | Differences between dorsal and ventral MCs

The results showed significant differences in the axonal projections of dorsal and ventral MCs. This is important because most investigators currently consider MCs to be a homogeneous population. In the past, there have been a few published papers where differences between dorsal and ventral MCs have been reported but they are rare. Therefore, our demonstration of significant differences in dorsal and ventral mouse MCs could have an impact on future investigations.

The past studies showing dorsal–ventral differences in MCs are mainly in the rat. For example, it has been shown that calretinin expression is high in ventral MC somata but not dorsal MCs (Freund & Buzsaki, 1996; Kosaka, Katsumaru, Hama, Wu, & Heizmann, 1987) a result we replicated in the present study. Another study that suggested that dorsal and ventral MCs were different was electrophysiological and used hippocampal slices to show that ventral MCs exhibited a greater degree of bursts in response to pharmacological agents (Jinno, Ishizuka, & Kosaka, 2003). More recently, a study in transgenic mice showed that ventral MCs have significantly different effects on behavior compared to dorsal MCs (Fredes et al., 2020).

The differences in dorsal versus ventral MCs are important because they may contribute to the dorsal and ventral differences in DG function that have been widely discussed (Chawla, Sutherland, Olson, McNaughton, & Barnes, 2018; Kheirbek et al., 2013; Kheirbek & Hen, 2011). The MC axon could play a role in these dorsal–ventral differences because dorsal MCs potentially innervate different parts of the GC apical dendrites. Another intriguing possibility is that dorsal and ventral MCs have different effects

on target neurons besides the GCs, for example, DG GABAergic neurons.

### 4.2 | Controls

The experimental data used many approaches to confirm the results. For example, two different transgenic mouse lines with Cre recombinase expressed in MCs were used. This study provides several lines of evidence that collectively suggest that the dorsal MCs differ from ventral MCs in their axonal projections throughout the septotemporal axis of the DG. Most notably, we found that the axons of dorsal MCs terminate in the IML and MML, depending on the level of the septotemporal axis. In contrast, ventral MCs did not share these characteristics, only showing terminations in the IML throughout the septotemporal axis.

A key factor to consider is contamination by GABAergic neurons of the DG that project to the MML, which have axons that collectively cover the GC somatodendritic axis (Freund & Buzsaki, 1996; Houser, 2007). However, there is no type of DG GABAergic neuron that projects only to the MML. Hilar GABAergic neurons which express somatostatin and NPY do have projections to the ML, but their axons are distributed to the MML and OML, and not the MML only (Deller & Leranth, 1990; Eyre & Bartos, 2019; Freund & Buzsaki, 1996; Houser, 2007; Sperk, Hamilton, & Colmers, 2007). ML GABAergic neurons such as MOPP cells (Halasy & Somogyi, 1993) or neurogliaform cells (Armstrong et al., 2011) may have an axon that is restricted to the ML but there are several characteristics about the axons of these GABAergic neurons that are different from the axonal distribution we observed in the MML. What we found was GFP+ axon terminals throughout the MML were robust from the lateral tip of the upper blade all the way around the DG to the lateral tip of the lower blade. In other words, a homogeneous band of fibers stained the MML throughout the DG in any given section. In contrast, the MOPP cell and neurogliaform cells have an axon that is localized to the area around their somata and this includes both the OML and MML (Armstrong et al., 2011; Halasy & Somogyi, 1993). Notably, the *Drd2-Cre* mouse has been suggested to show expression of Cre not only in MCs but also in some hippocampal GABAergic neurons (Puighermanal et al., 2015), but we have found this rare (Bernstein et al., 2020; Botterill et al., 2019). Nevertheless, in this article, we used two markers of GABAergic neurons and asked if there was colocalization of viral expression of MCs with GABAergic neuron labeling. The results did not show evidence of double-labeling, making it unlikely that there was significant contamination of GFP+ expression by GABAergic neurons.

It was particularly important to consider CA3 pyramidal cell axons in the ML because CA3 pyramidal cells project to the DG, although the axon terminals are mainly thought to innervate the hilus (Ishizuka, Weber, & Amaral, 1990; Scharfman, 2007a; Scharfman & Myers, 2012). Nevertheless, it has been reported that temporal CA3c pyramidal cells innervate the GCs by axons in the DG IML (Li et al., 1994). Notably, this work was done primarily in rat and it is

unclear whether the CA3 backprojection is similar in mice. We conducted control experiments that included expression in CA3c and found no evidence of axons in the MML. The expression in the IML appeared to be the same as mice where MCs were targeted specifically.

### 4.3 | Implications of differences in dorsal and ventral MC axons

The reason that differences in dorsal and ventral MCs are important is based on the past reports that the DG exhibits significant functional differences in dorsal and ventral regions. Some of these studies suggest that the dorsal DG has functions related to cognition and spatial navigation, whereas ventral DG has functions related to contextual conditioning, mood, and anxiety (Kheirbek & Hen, 2011). Given that the axons of dorsal MCs differ across the septotemporal axis, one possibility is that these axons may differentially influence GC activity in the dorsal and ventral hippocampus. In contrast, the axons of ventral MCs were always found in the IML and therefore should have very similar effects on the GCs they target, regardless of the position of the targeted cells in dorsal or ventral DG. As a result, the different projections across the septotemporal axis could give dorsal MCs the additional ability to encode information with a variable septotemporal valence. On the other hand, ventral MCs may have a more consistent, homogeneous function.

One of the ways that dorsal MCs may exert different effects on dorsal GCs than ventral GCs is that dorsal MCs potentially innervate a broader area of GC dendrites than ventral MCs. Another way that dorsal MCs may have different effects on dorsal GCs than ventral GCs is by contacting more of the different sublayers of the ML, leading to more opportunity to influence afferents to the GCs that lie in the MML. A functional interaction with the perforant path seems like an interesting possibility and a recent paper suggested that dorsal MC projections in the ventral DG can facilitate perforant path inputs to ventral GCs (Houser et al., 2020).

It is important to consider other targets of MCs, such as GABAergic neurons. In light of the results, more of the GABAergic neurons in the ML might be targeted in more ventral DG relative to more dorsal levels. This might lead to greater innervation by relatively dorsal MCs (compared with more ventral MCs) of GABAergic neurons which have most of their dendrites in the MML/OML. There also is more potential for axon-axon, glial, or other interactions in the ML for dorsal MCs than ventral MCs.

### 4.4 | MC axons are heterotopic rather than homotopic in the contralateral DG

Studies from the 1980s and 1990s based on markers such as *Phaseolus vulgaris* leucoagglutinin (PHAL), mainly in the rat, suggested that the axons of MCs were mainly destined for the IML in the ipsilateral hippocampus, terminating distal to the MC body (Scharfman & Myers, 2012). In addition, there was a homotopic distribution contralaterally, so dorsal MCs were

shown to project to the contralateral dorsal IML and ventral MCs projected to the contralateral ventral IML (Scharfman & Myers, 2012).

Since that time, no evidence has been provided that contradicts this idea of a homotopic contralateral projection. As a result, it is significant that the data in the present study show that MCs not only project homotopically in the contralateral DG, but also to heterotopic locations. Thus, a dorsal MC will project to distal ipsilateral locations, and to the majority of the septotemporal axis contralaterally. The exception could be the most ventral pole of the contralateral DG, because we found labeling relatively sparse in those locations.

Similarly, a ventral MC will project to the majority of the contralateral DG. Here the dorsal and ventral MCs may differ slightly because we found dorsal MCs projected to less of the septotemporal axis of the contralateral DG than ventral MCs. Together the data from dorsal and ventral MCs suggests a heterotopic distribution of the MC axon contralateral to its cell body and additional evidence that the dorsal and ventral MCs have a different axonal projection.

Why the present study found evidence of extensive contralateral projection, extending not just homotopically but throughout the contralateral septotemporal axis, is likely to be due to technical reasons. Previous studies that characterized the commissural axon either used bulk injection of agents like PHAL, or used biocytin-labeling of intracellularly recorded MCs (Buckmaster et al., 1996; for review see Scharfman & Myers, 2012). PHAL and biocytin may simply be limited in their ability to reveal the extent of contralateral projections of MCs. In contrast, selective transgenic lines and viral constructs tagged with fluorescent fluorophores appear to label MCs far more extensively and comprehensively. However, the majority of studies that have used viral injections or reporter lines to study MCs have focused on somata rather than axonal projections (Azevedo et al., 2019; Bui et al., 2018; Danielson et al., 2017; Senzai & Buzsaki, 2017; Yeh et al., 2018).

The significance of the more widespread contralateral projection is interesting to consider. One possibility is that a more widespread axon makes MCs able to interconnect more lamellae of the DG. As such, MCs are more likely to serve roles that have been suggested for them before, such as a role as a sentinel cell, “broadcasting” its input to numerous GCs at almost all levels of the DG (Scharfman, 2016). The idea that MCs detect what is novel about the environment and send that to GCs so that environmental context can be processed has been suggested (Bernstein, Lu, Botterill, & Scharfman, 2019; Duffy, Schaner, Chin, & Scharfman, 2013), and could make it important for MCs to send their axons to all parts of the DG.

### 4.5 | Blade differences

A notable feature of this work is that we evaluated potential differences in the MC axon across the different parts of the DG, including the upper blade, crest, and lower blade. Our analysis revealed that the distance between the GCL and the GFP+ axon was often largest in the upper blade, regardless of the site of viral injection in the dorsal or ventral DG. The importance of these differences is not clear, although more and more are being detected that is distinct about the different

blades of the DG (Chawla et al., 2005; Scharfman, Sollas, Smith, Jackson, & Goodman, 2002; Schmidt, Marrone, & Markus, 2012).

## 4.6 | Limitations

Although we did not observe any sex differences in the present study, the possibility of sex differences is notable because of prior publications about sex differences in MCs (Guidi, Severi, Ciani, & Bartesaghi, 2006) and because we recently reported sex differences in the behavioral effects of MC excitation and inhibition (Botterill et al., 2021).

## 5 | CONCLUSIONS

The results show that dorsal and ventral MCs of the adult C57BL/6 mouse differ in their axonal projections. Notably, the axons of dorsal MCs have a unique axonal projection pattern that differs depending on the level of the septotemporal axis of the DG. In contrast, the axons of ventral MCs are primarily restricted to the IML throughout the DG. The findings were thoroughly tested to confirm their reproducibility and lack of confounding factors. The implications are that the dorsal MCs may influence the processing of information in the DG differently than ventral MCs. Dorsal–ventral differences in MCs could therefore contribute to dorsal–ventral differences of the DG.

### ACKNOWLEDGEMENTS

We thank members of the Scharfman lab for their helpful comments and suggestions. This work was supported by the New York State Office of Mental Health and NIH R01 MH-109305 to Helen E. Scharfman. Justin J. Botterill was supported by a postdoctoral fellowship from the American Epilepsy Society (AES).

### AUTHOR CONTRIBUTIONS

*Conceptualization:* Justin J. Botterill, Helen E. Scharfman; *Data collection and analysis:* Justin J. Botterill, Kathleen J. Gerencer, K. Yaragudri Vinod, David Alcantara-Gonzalez. *Wrote the manuscript:* Justin J. Botterill and Helen E. Scharfman. All authors reviewed and approved the manuscript.

### CONFLICT OF INTEREST

The authors declare that the research was conducted in the absence of any commercial or financial interests that could be construed as a potential conflict of interest.

### DATA AVAILABILITY STATEMENT

Further information and requests for reagents or resources should be directed to and will be fulfilled by the corresponding author, Dr. Helen Scharfman (helen.scharfman@nki.rfmh.org).

### ORCID

Justin J. Botterill  <https://orcid.org/0000-0002-3141-2281>

David Alcantara-Gonzalez  <https://orcid.org/0000-0002-1944-6163>

## REFERENCES

- Amaral, D. G., Scharfman, H. E., & Lavenex, P. (2007). The dentate gyrus: Fundamental neuroanatomical organization (dentate gyrus for dummies). *Progress in Brain Research*, 163, 3–22.
- Armstrong, C., Szabadics, J., Tamas, G., & Soltesz, I. (2011). Neurogliaform cells in the molecular layer of the dentate gyrus as feed-forward gamma-aminobutyric acidergic modulators of entorhinal-hippocampal interplay. *The Journal of Comparative Neurology*, 519, 1476–1491.
- Azevedo, E. P., Pomeranz, L., Cheng, J., Schneeberger, M., Vaughan, R., Stern, S. A., ... Friedman, J. M. (2019). A role of Drd2 hippocampal neurons in context-dependent food intake. *Neuron*, 102, 873–886.e875.
- Bernstein, H. L., Lu, Y. L., Botterill, J. J., Duffy, A. M., LaFrancois, J., & Scharfman, H. (2020). Excitatory effects of dentate gyrus mossy cells and their ability to influence granule cell firing: an optogenetic study in adult mouse hippocampal slices. *bioRxiv*, 1–105. <https://doi.org/10.1101/2020.06.06.137844>
- Bernstein, H. L., Lu, Y. L., Botterill, J. J., & Scharfman, H. E. (2019). Novelty and novel objects increase c-Fos immunoreactivity in mossy cells in the mouse dentate gyrus. *Neural Plasticity*, 2019, 1815371.
- Blasco-Ibanez, J. M., & Freund, T. F. (1997). Distribution, ultrastructure, and connectivity of calretinin-immunoreactive mossy cells of the mouse dentate gyrus. *Hippocampus*, 7, 307–320.
- Botterill, J. J., Guskjolen, A. J., Marks, W. N., Caruncho, H. J., & Kalynchuk, L. E. (2015). Limbic but not non-limbic kindling impairs conditioned fear and promotes plasticity of NPY and its Y2 receptor. *Brain Structure & Function*, 220, 3641–3655.
- Botterill, J. J., Lu, Y. L., LaFrancois, J. J., Bernstein, H. L., Alcantara-Gonzalez, D., Jain, S., ... Scharfman, H. E. (2019). An excitatory and epileptogenic effect of dentate gyrus mossy cells in a mouse model of epilepsy. *Cell Reports*, 29, 2875–2889.e2876.
- Botterill, J. J., Nogovitsyn, N., Caruncho, H. J., & Kalynchuk, L. E. (2017). Selective plasticity of hippocampal GABAergic interneuron populations following kindling of different brain regions. *The Journal of Comparative Neurology*, 525, 389–406.
- Botterill, J. J., Vinod, K. Y., Gerencer, K. J., Teixeira, C. M., LaFrancois, J. J., & Scharfman, H. E. (2021). Bidirectional regulation of cognitive and anxiety-like behaviors by dentate gyrus mossy cells in male and female mice. *The Journal of Neuroscience* in press. JN-RM-1724-20.
- Buckmaster, P. S., & Schwartzkroin, P. A. (1994). Hippocampal mossy cell function: A speculative view. *Hippocampus*, 4, 393–402.
- Buckmaster, P. S., Wenzel, H. J., Kunkel, D. D., & Schwartzkroin, P. A. (1996). Axon arbors and synaptic connections of hippocampal mossy cells in the rat in vivo. *The Journal of Comparative Neurology*, 366, 271–292.
- Bui, A. D., Nguyen, T. M., Limouse, C., Kim, H. K., Szabo, G. G., Felong, S., ... Soltesz, I. (2018). Dentate gyrus mossy cells control spontaneous convulsive seizures and spatial memory. *Science*, 359, 787–790.
- Chawla, M. K., Guzowski, J. F., Ramirez-Amaya, V., Lipa, P., Hoffman, K. L., Marriott, L. K., ... Barnes, C. A. (2005). Sparse, environmentally selective expression of arc RNA in the upper blade of the rodent fascia dentata by brief spatial experience. *Hippocampus*, 15, 579–586.
- Chawla, M. K., Sutherland, V. L., Olson, K., McNaughton, B. L., & Barnes, C. A. (2018). Behavior-driven arc expression is reduced in all ventral hippocampal subfields compared to CA1, CA3, and dentate gyrus in rat dorsal hippocampus. *Hippocampus*, 28, 178–185.
- Danielson, N. B., Turi, G. F., Ladow, M., Chavlis, S., Petranonakis, P. C., Poirazi, P., & Losonczy, A. (2017). In vivo imaging of dentate gyrus mossy cells in behaving mice. *Neuron*, 93, 552–559.e554.
- Deller, T., & Leranath, C. (1990). Synaptic connections of neuropeptide Y (NPY) immunoreactive neurons in the hilar area of the rat hippocampus. *The Journal of Comparative Neurology*, 300, 433–447.
- Duffy, A. M., Schaner, M. J., Chin, J., & Scharfman, H. E. (2013). Expression of c-fos in hilar mossy cells of the dentate gyrus in vivo. *Hippocampus*, 23, 649–655.

- Eyre, M. D., & Bartos, M. (2019). Somatostatin-expressing interneurons form axonal projections to the contralateral hippocampus. *Frontiers in Neural Circuits*, 13, 56.
- Fredes, F., Silva, M. A., Koppensteiner, P., Kobayashi, K., Joesch, M., & Shigemoto, R. (2020). Vento-dorsal hippocampal pathway gates novelty-induced contextual memory formation. *Current Biology*, 31(1), 25–38.e5.
- Freund, T. F., & Buzsaki, G. (1996). Interneurons of the hippocampus. *Hippocampus*, 6, 347–470.
- Fujise, N., Liu, Y., Hori, N., & Kosaka, T. (1998). Distribution of calretinin immunoreactivity in the mouse dentate gyrus: II. Mossy cells, with special reference to their dorsoventral difference in calretinin immunoreactivity. *Neuroscience*, 82, 181–200.
- Guidi, S., Severi, S., Ciani, E., & Bartesaghi, R. (2006). Sex differences in the hilar mossy cells of the Guinea-pig before puberty. *Neuroscience*, 139, 565–576.
- Haery, L., Deverman, B. E., Matho, K. S., Cetin, A., Woodard, K., Cepko, C., ... Fan, M. (2019). Adeno-associated virus technologies and methods for targeted neuronal manipulation. *Frontiers in Neuroanatomy*, 13, 93.
- Halasy, K., & Somogyi, P. (1993). Subdivisions in the multiple GABAergic innervation of granule cells in the dentate gyrus of the rat hippocampus. *The European Journal of Neuroscience*, 5, 411–429.
- Han, Z. S., Buhl, E. H., Lorinczi, Z., & Somogyi, P. (1993). A high degree of spatial selectivity in the axonal and dendritic domains of physiologically identified local-circuit neurons in the dentate gyrus of the rat hippocampus. *The European Journal of Neuroscience*, 5, 395–410.
- Houser, C. R. (2007). Interneurons of the dentate gyrus: An overview of cell types, terminal fields and neurochemical identity. *Progress in Brain Research*, 163, 217–232.
- Houser, C. R., Peng, Z., Wei, X., Huang, C. S., & Mody, I. (2020). Mossy cells in the dorsal and ventral dentate gyrus differ in their patterns of axonal projections. *The Journal of Neuroscience*, 41(5), 991–1004.
- Ishizuka, N., Weber, J., & Amaral, D. G. (1990). Organization of intrahippocampal projections originating from CA3 pyramidal cells in the rat. *The Journal of Comparative Neurology*, 295, 580–623.
- Jinde, S., Zsiros, V., Jiang, Z., Nakao, K., Pickel, J., Kohno, K., ... Nakazawa, K. (2012). Hilar mossy cell degeneration causes transient dentate granule cell hyperexcitability and impaired pattern separation. *Neuron*, 76, 1189–1200.
- Jinno, S., Ishizuka, S., & Kosaka, T. (2003). Ionic currents underlying rhythmic bursting of ventral mossy cells in the developing mouse dentate gyrus. *The European Journal of Neuroscience*, 17, 1338–1354.
- Jung, D., Kim, S., Sariev, A., Sharif, F., Kim, D., & Royer, S. (2019). Dentate granule and mossy cells exhibit distinct spatiotemporal responses to local change in a one-dimensional landscape of visual-tactile cues. *Scientific Reports*, 9, 9545.
- Kheirbek, M. A., Drew, L. J., Burghardt, N. S., Costantini, D. O., Tannenholz, L., Ahmari, S. E., ... Hen, R. (2013). Differential control of learning and anxiety along the dorsoventral axis of the dentate gyrus. *Neuron*, 77, 955–968.
- Kheirbek, M. A., & Hen, R. (2011). Dorsal vs ventral hippocampal neurogenesis: Implications for cognition and mood. *Neuropsychopharmacology*, 36, 373–374.
- Kosaka, T., Katsumaru, H., Hama, K., Wu, J. Y., & Heizmann, C. W. (1987). GABAergic neurons containing the Ca<sup>2+</sup>-binding protein parvalbumin in the rat hippocampus and dentate gyrus. *Brain Research*, 419, 119–130.
- Lanciego, J. L., & Wouterlood, F. G. (2020). Neuroanatomical tract-tracing techniques that did go viral. *Brain Structure & Function*, 225, 1193–1224.
- Li, X. G., Somogyi, P., Ylinen, A., & Buzsaki, G. (1994). The hippocampal CA3 network: An in vivo intracellular labeling study. *The Journal of Comparative Neurology*, 339, 181–208.
- Myers, C. E., & Scharfman, H. E. (2009). A role for hilar cells in pattern separation in the dentate gyrus: A computational approach. *Hippocampus*, 19, 321–337.
- Oh, S. J., Cheng, J., Jang, J. H., Arace, J., Jeong, M., Shin, C. H., ... Oh, Y. S. (2019). Hippocampal mossy cell involvement in behavioral and neurogenic responses to chronic antidepressant treatment. *Molecular Psychiatry*, 25, 1215–1228.
- Puighermanal, E., Biever, A., Espallergues, J., Gangarossa, G., De Bundel, D., & Valjent, E. (2015). drd2-cre:Ribotag mouse line unravels the possible diversity of dopamine d2 receptor-expressing cells of the dorsal mouse hippocampus. *Hippocampus*, 25, 858–875.
- Scharfman, H. E. (2007a). The CA3 "backprojection" to the dentate gyrus. *Progress in Brain Research*, 163, 627–637.
- Scharfman, H. E. (2007b). *The dentate gyrus: A comprehensive guide to structure, function, and clinical implications*. Amsterdam: Elsevier.
- Scharfman, H. E. (2016). The enigmatic mossy cell of the dentate gyrus. *Nature Reviews. Neuroscience*, 17, 562–575.
- Scharfman, H. E. (2017). Advances in understanding hilar mossy cells of the dentate gyrus. *Cell and Tissue Research*, 373, 643–652.
- Scharfman, H. E., & Myers, C. E. (2012). Hilar mossy cells of the dentate gyrus: A historical perspective. *Frontiers in Neural Circuits*, 6, 106.
- Scharfman, H. E., Sollas, A. L., Smith, K. L., Jackson, M. B., & Goodman, J. H. (2002). Structural and functional asymmetry in the normal and epileptic rat dentate gyrus. *The Journal of Comparative Neurology*, 454, 424–439.
- Schmidt, B., Marrone, D. F., & Markus, E. J. (2012). Disambiguating the similar: The dentate gyrus and pattern separation. *Behavioural Brain Research*, 226, 56–65.
- Senzai, Y., & Buzsaki, G. (2017). Physiological properties and behavioral correlates of hippocampal granule cells and mossy cells. *Neuron*, 93, 691–704.
- Sperk, G., Hamilton, T., & Colmers, W. F. (2007). Neuropeptide Y in the dentate gyrus. *Progress in Brain Research*, 163, 285–297.
- Yeh, C. Y., Asrican, B., Moss, J., Quintanilla, L. J., He, T., Mao, X., ... Song, J. (2018). Mossy cells control adult neural stem cell quiescence and maintenance through a dynamic balance between direct and indirect pathways. *Neuron*, 99, 493–510.e494.

## SUPPORTING INFORMATION

Additional supporting information may be found online in the Supporting Information section at the end of this article.

**How to cite this article:** Botterill JJ, Gerencer KJ, Vinod KY, Alcantara-Gonzalez D, Scharfman HE. Dorsal and ventral mossy cells differ in their axonal projections throughout the dentate gyrus of the mouse hippocampus. *Hippocampus*. 2021; 31:522–539. <https://doi.org/10.1002/hipo.23314>